Thermal behaviour and heat capacity of ionic liquids: benzilimidazolium and alkylimidazolium derivatives

Paulo Bruno Pontes Serra

Mestrado em Química
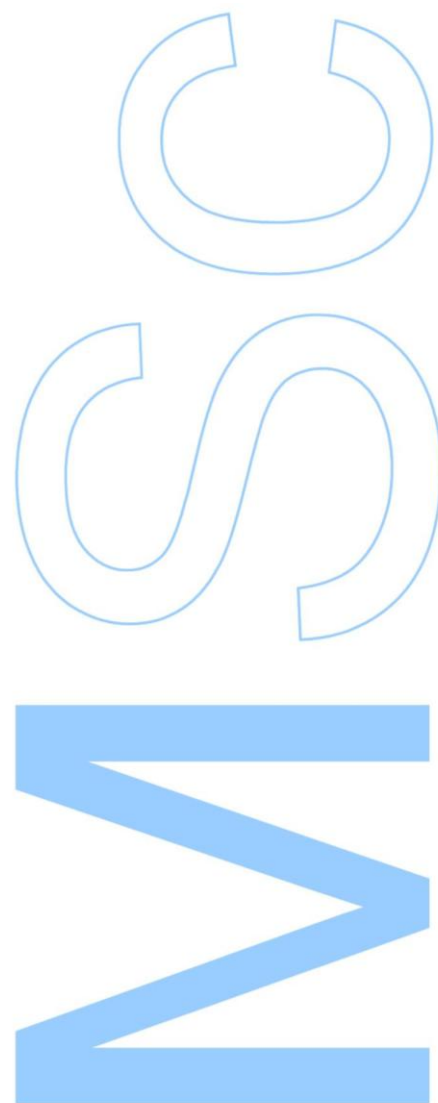Departamento de Química e Bioquímica
2012/2013

Supervisor
Luís Manuel das Neves Belchior Faia dos Santos
Professor associado,
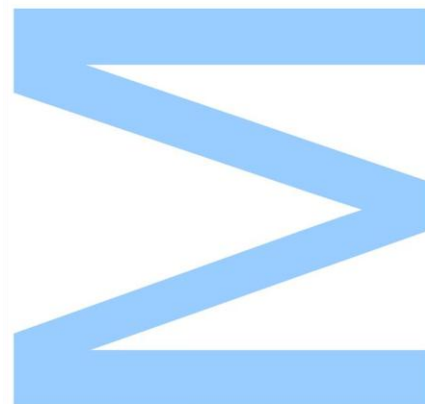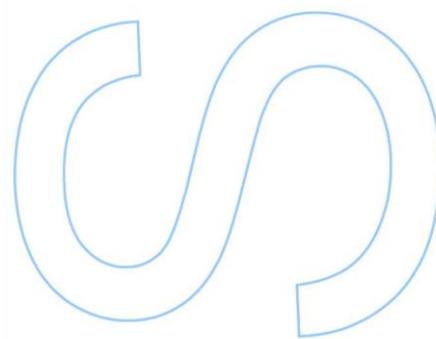Faculdade de Ciências da Universidade do Porto.

FCUP

Thermal behaviour and heat capacity of ionic liquids: benzilimidazolium and alkylimidazolium derivatives

U. PORTO

FC **FACULDADE DE CIÊNCIAS**
UNIVERSIDADE DO PORTO

Todas as correções determinadas pelo júri, e só essas, foram efetuadas.

O Presidente do Júri,

Porto, _____/_____/_____
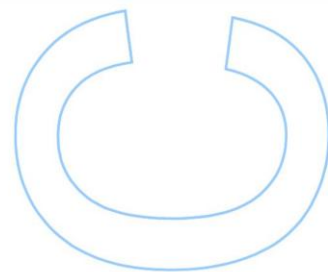
FCUP
Thermal behaviour and heat capacity of ionic liquids: benzilimidazolium and alkylimidazolium derivatives

Acknowledgements

I would like to thank all the support provided by Professor Fulem and Professor Růžička, along my internship in ICT Prague. If I had a successful stay, it was due to their support along the eight months lived in Prague.

I would also like to thank all my friends that I met in Prague. They provided a great experience that I will carry with me for the rest of my life.

Agradecimentos

Gostaria de agradecer a todas as pessoas que trabalharam comigo de perto e que me ajudaram a criar este trabalho. Gostaria de realçar, nomeadamente, o Professor Luís Santos pela sua dedicação e apoio prestado, também à Marisa Rocha por toda a sua disponibilidade e apoio prestado e ao Filipe Ribeiro por todos os seus conselhos. Também gostaria de agradecer aos meus amigos da Faculdade de Ciências da Universidade do Porto que me acompanharam e apoiaram durante todos estes anos de estudo.

Por fim, gostaria de agradecer à minha família e restantes amigos que me ajudaram a tornar no homem que sou hoje.

Thermal behaviour and heat capacity of ionic liquids: benzilimidazolium and alkylimidazolium derivatives

Resumo

Este trabalho foca o estudo térmico, a medição de capacidades caloríficas em fase condensada e o estudo de transições de fase de líquido iónicos. Foram estudadas dua famílias de líquidos iónicos, uma baseada no catião 1-benzil-3-metilimidazólio conjugado com quatro aniões (tetrafluoroborato; hexafluorofosfato; 1,1,2,2-tetrafluoroetanossulfonato; bis(trifluorometilsulfonil)imida) e a série 1-alquil-3-metilimidazólio: metil, -etil, -propil, -butil, -pentil, -hexil. –heptil, -octil, -nonil, -decanil and -dodecanil-3-metilimidazólio com o anião hexafluorofosfato.

O efeito de diferentes aniões na presença de um catião comum foi estudado na série do 1-benzil-3-metilimidazólio, assim como o impacto do comprimento da cadeia alquílica no catião da série do 1-alquil-3-metilimidazólio.

O estudo térmico, cristalinidade, temperatura de vitrificação, estudo de transições de fase sólido-sólido e fusão, foram investigadas por calorimetria diferencial de varrimento na gama de temperaturas de 183 K a 423 K. Com base nos resultados obtidos foram derivadas as entalpias e entropias das transições de fase mais relevantes. As capacidades caloríficas das fases condensadas foram medidas usando o método contínuo e de salto de temperatura no intervalo de temperaturas de 253 K a 353 K por microcalorimetria diferencial de varrimento.

Os resultados obtidos para temperaturas de transições de fase e capacidades caloríficas foram comparados com valores da literatura e com métodos de estimativa de contribuição de grupos. Adicionalmente, é ainda apresentada uma análise comparativa do efeito do anião nos líquidos iónicos derivados do 1-benzil-3-metilimidazólio, assim como o efeito do grupo benzil. O efeito do tamanho da cadeia alquílica é explorado nas propriedades da série 1-alquil-3-metilimidazólio hexafluorofosfato.

Abstract

This work is focused on the thermal study, condensed phases heat capacities measurements and phase behaviour studies of ionic liquids. It was studied two families, one based on the 1-benzyl-3-methylimidazolium cation conjugated with 4 anions (tetrafluoroborate; hexafluorophosphate; 1,1,2,2-tetrafluoroethanesulfonate; bis(trifluoromethylsulfonyl)imide), and the 1-alkyl-3-methylimidazolium series: -methyl; -ethyl; -propyl; -butyl; -pentyl; -hexyl; –heptyl; -octyl; -nonyl; -decyl and -dodecyl-3-methylimidazolium with the anion hexafluorophosphate.

The effect of the anion considering a common cation was explored for the 1-benzyl-3-methylimidazolium based ionic liquids, and additionally, it was evaluated the impact of the alkyl side chain in the 1-alkyl-3-methylimidazolium hexafluorophosphate ionic liquid series.

The thermal study, crystallinity, glass transition temperature, solid-solid phase transitions and melting studies, were investigated by the differential scanning calorimeter in the temperature range from 183 K to 423 K. With the obtained results, the most relevant transitions enthalpy and entropy were derived. The heat capacities of the condensed phases were measured by continuous and step method in the temperature interval from 253 K to 353 K by differential scanning microcalorimeter.

The obtained results for phase transitions temperatures and heat capacities were compared with available literature values as well as with group contribution estimation methods. A comparative analysis of the anion effect in the 1-benzyl-3-methylimidazolium ionic liquids, and the benzyl group effect is also presented. The alkyl side chain length effect on the properties of 1-alkyl-3-methylimidazolium series is explored.

Index

| **FCUP**
Thermal behaviour and heat capacity of ionic liquids: benzilimidazolium and
alkylimidazolium derivatives

Figure Index

Table index

Abbreviations list

ILs - Ionic Liquids

DSC - Differential Scanning Calorimetry

T_g - Glass transition temperature

T_{s-s} – Solid-solid transition temperature

T_m - Melting temperature

T_{cc} – Cold crystallization temperature

c_p – Specific heat capacity at constant pressure

$C_{p,m}$ – Molar heat capacity at constant pressure

C_p^{lf} – Heat capacity at constant pressure from linear fit

C_p^{exp} – Heat capacity at constant pressure experimental

GCM – group contribution method

RTILs – Room temperature ionic liquids

MALDI - Matrix-assisted laser desorption/ionization

TOF - Time-of-flight mass spectrometer

GC – Gas chromatography

ΔH – Enthalpy variation

ΔT – Temperature variation

T - Temperature

ΔS – Entropy variation

ΔG – Gibbs energy variation

mW – Milliwatt

CAS number – Chemical abstracts service number

dev. – deviation

eq. – Equation

J – Joule

g - gram

K – Kelvin

n [C] – number of Carbons in the alkyl chain

s – second

exp – experimental

lit – literature

1. Introduction

1.1. General introduction

This thesis is based on the work performed in the Faculty Vysoká Škola Chemicko-Technologická v Praze, VSCHT, in Prague. Along the 8 months of the Erasmus placement, the phase transitions and heat capacities of several ionic liquids were studied with the collaboration of Professor Michal Fulem and Professor Květoslav Růžička.

1.2. Motivation and Aim of the Work

The present work is focused on the thermodynamics of phase transitions and heat capacities of the condensed phases of some ionic liquids. The studied samples are based on imidazolium cation. This organic cation features some interesting properties that lead to its family study [1]:

- thermal and electrochemical stability;
- wide liquidus range;
- low reactivity with water;
- low viscosity;
- solvent properties adjustment.

Two variations of this cation were chosen, allowing the work division in two parts and to study different properties. The first group possesses a bulky variation of the cation: the 1-Benzyl-3-methylimidazolium (Figure 1.1) with each nitrogen connected with distinct groups. In one, a methyl group is connected (small size) and in the other a benzyl group is bonded (a bulky group) as seen in Figure 1.1. Those features lead to a delocalization in the cation charge and a big asymmetry. This cation was tested with 4 different anions that are commonly used nowadays: two small sized and symmetric inorganic anions, the BF_4 and PF_6; and two big sized

asymmetric organic anions, $C_2F_4HSO_3$ and NTf_2. These anions were chosen so their effect in the heat capacities and phase transitions could be studied.
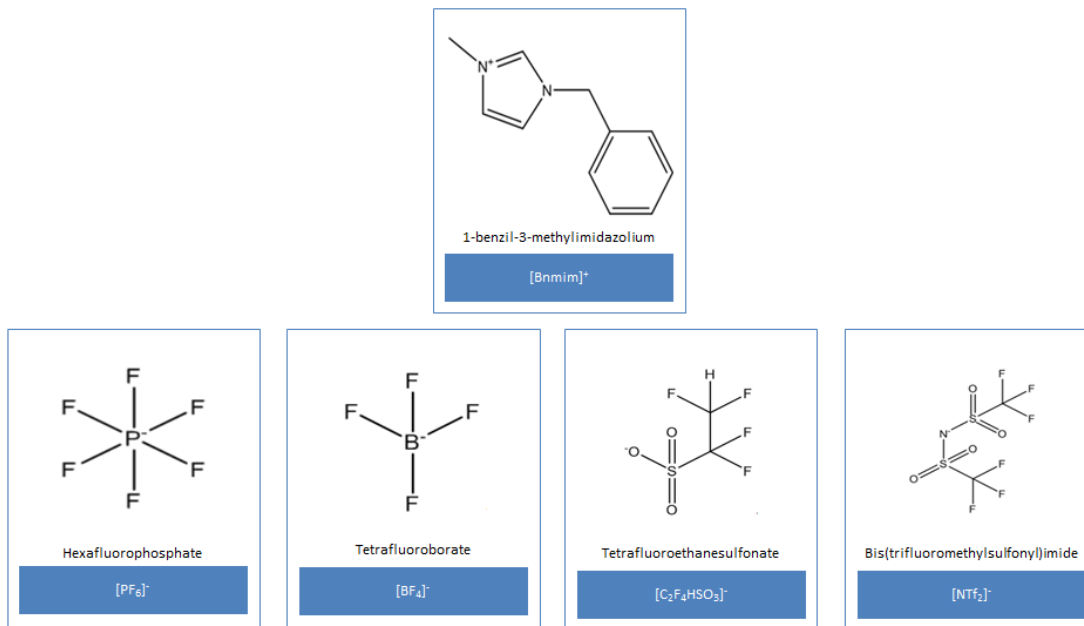
Figure 1.1 - Schematic structural formula of the cation 1-benzyl-3-methylimidazolium and the anions: hexafluorophosphate; tetrafluoroborate; tetrafluoroethanesulfonate; bis(trifluoromethylsulfonyl)imide.

The second family of ILs has a similar cation, changing the benzyl group by an alkyl chain with different lengths: -methyl, -ethyl, -propyl, -butyl, -pentyl, -hexyl. –heptyl, -octyl, -nonyl, -decyl and -dodecyl-3-methylimidazolium. The different alkyl chains presence will influence the cation charge localization. In this case, the cation was only tested with one anion, the PF_6, so the effect of the alkyl side chain on the properties of this ionic liquids series could be studied. The obtained results were compared with the ones for the $[C_nC_1][PF_6]$ measured in Porto, in order to evaluate the change of the anion considering the same cation. Figure 1.2 shows the general structure of this IL family.
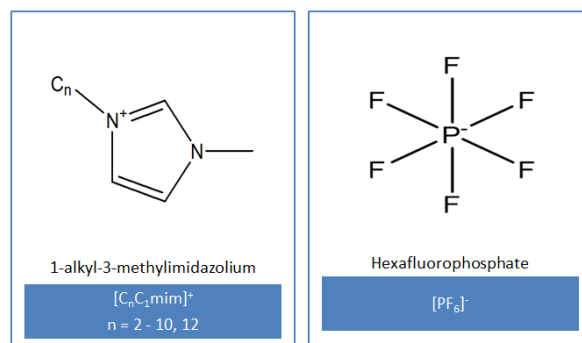
Figure 1.2 - Schematic structural formula of the cation 1-alkyl-3-methylimidazolium and the anion, hexafluorophosphate.

So, the main goal of this work is to use the obtained results from the heat capacity and thermal analysis of the ionic liquids under studies, to get more insights about the:

- the influence of different anions in the 1-benzyl-3-methylimidazolium based ionic liquids;
- the effect of the alkyl chain length in the 1-alkyl-3- methylimidazolium hexafluorophosphate series and evaluate the linearity in the heat capacity along the alkyl side chain length.

Additionally, the heat capacity results obtained for the 1-alkyl-3-methylimidazolium hexafluorophosphate ionic liquids will be compared with the data measured in the University of Porto for the 1-alkyl-3-methylimidazolium bis(trifluoromethylsulfonyl)imide, in order to explore the effect of the anion on the studied properties.

1.3. The ionic liquids

Ionic liquids (ILs) are salts composed by an organic cation and an inorganic or organic anion. They usually are liquids at room temperature, with melting points usually below 373 K. The ILs with melting points around or below room temperature are also denominated "Room Temperature Ionic Liquids" (RTILs)[2].

The large quantity of known ions, allows the formation of many different ILs with different characteristics. Those characteristics are deeply influenced by the anion/cation pair choice, and also by their size. Since the cation is usually bigger than the anion, this leads to complex structural organizations in order to maintain the electroneutrality conditions from the cation/anion aggregation. This aggregation can also be affected by neutrally charged structures, such as alkyl chains that, when present (usually attached to the cation), are repelled by the charged zones of the cation/anion, creating nano-structures with low-charge density molecular residues [3]:

- In "islands" format – when the alkyl chain is small, creating non charged "islands" in the charged "sea". Here the main interaction is electrostatic;

- In channels format – when the alkyl chain is big, creating channels formed by alkyl chains in one side and a charged zone in the other side. The main observed interaction is Van der Waals.

The different charged zones in the ILs leads to weaker interionic interactions and less ion-ion packing in the crystal cell [4, 5] explaining their low melting points, for example.

Another important feature is their thermal stability. They are in liquid state over a wide temperature range, and in general they don't reach gas phase, being limited by the thermal decomposition temperature, due to the organic structures presented. Also, some of them don't even crystallize, staying in a metastable equilibrium after the glass transition.

Other properties such as viscosity, heat capacity, conductivity, can be adjusted just by selecting a defined anion/cation pair. This is due to their easiness in changing the cation/anion combination, allowing to easily tune their properties, achieving desired characteristics. The alkyl chain size also plays a role here, since it can make the ILs more or less viscous or can lower or increase the melting point and/or other properties, which are important features for industrial applications.

1.3.1. Characteristics and applications of ionic liquids

Ionic liquids were chosen since there is information about just some of them and, so far, some interesting properties are known – that they are liquid over a wide range of temperatures and they are able to dissolve both organic and inorganic liquids [6, 7] It is also supported that they can lead to enhanced reaction rates, higher yields and change selectivities in chemical reactions [8].

Other ILs properties are also known, leading to the growing interest in their study:

- Low vapour pressure – low mass loss by vaporization, good for environment;
- Electric conductivity – important for new batteries development;
- Biphasic systems possible;
- Liquid crystalline structures;
- High electroelasticity - electric fields can induce deformations in the IL;
- Thermal stability ;
- High heat capacity – capacity to sustain large amounts of heat, important for industry;
- Non flammability – due to their low vapour pressure;
- Environmentally safe compounds.

From all the properties mentioned before, some ILs applications in different fields are being suggested:

- Electrolytes - fuel cells, sensors, batteries, supercapacitors, metal finishing, and coating [9];
- Heat storage and thermal fluids [10];
- Liquid crystals, image devices [11];
- Solvents - nano-particle-synthesis and polymerization [12];
- Analytics - MALDI-TOF-matrices [13],GC-head-space-solvents [14];
- Lubricants and additives - lubricants and fuel additives [15];
- Separation - gas separation [16], extractive distillation [17], extraction [18], and membranes [19].

1.4. Calorimetry

Calorimetry is the science that measures heat exchanges. For this purpose a proper system was created, the calorimeter. The calorimeter is used to exactly determine the amount of heat used to affect the temperature of a sample, or the heat exchange occurring in chemical reactions. Calorimeter methods may be classified by the measurement principle (heat compensation) or operating method (static, flow or scanning) or construction principle (single or twin cell) [20].

According with the experimental field, multiple kinds of calorimeters were developed such as [21]:

- Drop calorimeters, to determine mean heat capacities or enthalpy differences;
- Differential Scanning Calorimetry or the Differential Thermal analysis – two similar techniques used to analyse the thermodynamic properties of a sample for a determined temperature range;
- Bomb calorimeters, to determine combustion heats;
- Gas calorimeters, used for the continuous or discontinuous measurement of the calorific value of fuel gases;
- Isoperibol mixing calorimeters, to investigate the reaction heats resulting from mixing two fluids, or a fluid and a solid.

The goal of this work is the study of the ILs thermal behavior and heat capacities, so the calorimeters used were Differential Scanning Calorimeters, or DSC's. The DSC measures the change of the difference in the heat flow rate to the sample and to a reference while they are subjected to a controlled temperature program.

1.5. Differential Scanning calorimetry, DSC

The Differential Scanning calorimetry, or DSC, is a calorimeter where the sample is submitted to a controlled temperature program and its behaviour is recorded for phase transition analysis and heat capacity calculation [7]. For the measurement, the sample is inserted in a metallic pan (usually aluminium or platinum, to allow a fast heat transfer between the sample and its surroundings) and well closed to avoid mass loss along measurements.

Along the measurements, the results are affected by the pan heat retention and to remove this effect, an empty reference pan is used along the sample measurement. This reference pan can be in the same furnace as the sample or in a separate one, distinguishing the two different DSCs:

- Power compensation DSC – sample and reference are separated and the power measurement is done by comparison between difference of energy supply to the sample and reference cavities;
- Heat Flow DSC – sample and reference share the same furnace and the power measurement is based in the incoming/outcoming - heat flow difference between the sample and the reference cell.

The DSC's are commonly used in the development, quality and process control in many industrial fields and for thermal characterization of construction materials, polymeric materials, composites, chemicals and pharmaceuticals etc. [21].

DSC can be used as a tool for:

- Thermal behaviour;
- Phase transitions analysis;
- Heat capacity measurements;
- Process Enthalpy and Entropy evaluations;
- Studies about the heat generation in biological systems.

In the studies of ILs, two different DSC's were used: a TA Instruments Q1000 DSC (used in phase transitions analysis) and a Setaram µDSCIIIa (for the heat capacity determination).

1.6. The Differential Scanning Calorimeters

In the ILs studies, two different DSC were used: a TA Instruments Q1000 DSC (for phase transitions analysis, Figure 1.3) and a Setaram μDSCIII (for heat capacity determinations, Figure 1.5).

1.6.1. TA Instruments Q1000

Figure 1.3 - The TA Instruments Q1000 used in this work for phase transitions measurements.

The measurements with the TA Instruments Q1000 were performed using a continuous method, using a linear heating rate of 3 K•min^{-1}, from 183 K to 403 K. Two isothermal delays of 1800 s were used in the beginning and at the end of the measurement to allow the DSC signal and sample stabilization (ionic liquids are deeply affected by their thermal history which depending on the heating/cooling rate induces different types of crystallization, so to avoid the study of different crystal phases the sample is put under a high cooling rate and stabilized before beginning the heating for thermal analysis). The pans used in the TA Instruments Q1000 are aluminum made, and are depicted in Figure 1.4

Figure 1.4 – The 10 mm^3 Tzero series hermetic pans used in the TA Instruments Q1000.

This calorimeter used a technical nitrogen gas flow (from SIAD Czech Company) with a guaranteed purity (from the producer) of more than 99.99% (the gas flow used was around 50 mL•min^{-1}).

Other characteristics from this heat flow DSC are listed below [22]:

- Temperature range from 183 K- 673 K;

- Temperature Accuracy of 0.1 K;

- Temperature Precision of 0.05 K;

- Calorimetric Precision (metal standards) of 1%;

- Power sensitivity of 0.2 μW;

- 50-position autosampler;

- Digital mass flow controller.

1.6.2. Setaram μDSC IIIa

Figure 1.5 - The Setaram μDSC IIIa used in this work for heat capacities measurements.

The liquid heat capacity was measured with a Setaram μDSC IIIa, in the range from 273 to 355 K and used the incremental temperature mode for the step method (described in chapter 1.7.2). Each 5 K step included a heating rate of 0.3 K•min^{-1} was used, between two isothermal delays of 2600 s. For continuous method, a heating rate of 0.3 K·min^{-1} was used, between two isothermal delays of 2600 s. Obtained data was integrated using the Setaram software package SetSoft 2000. The typical mass of samples was 0.4 g to 1 g.

The combined expanded uncertainty of the ICT heat capacity measurements is estimated to be $U_c(C_{p,m}) = 0.01 \ C_{p,m}$. [23], the measuring procedure was described in detail in Fulem *et al* [24].

In Figure 1.6 are presented the closed Hastelloy C (majorly made by Nickel, Chromium and Molybdenum) vessels, with volume of 1 cm^3, used in the Setaram μDSC IIIa.

Figure 1.6 - The μDSC vessels used in the Setaram μDSC IIIa.

The temperature of the calorimeter is regulated by means of a cooled water bath.

The Setaram µDSC IIIa presents characteristics such as [22]:

- Temperature range from 253 - 393 K;

- Scanning rate from 0.001 K•min^{-1} to 1.2 K•min^{-1} in the whole temperature range;

- Detection limit from 0.2 until 2 µW;

- Resolution of 40 nW;

- Two scanning modes - Isothermal and differential.

1.7. Heat capacity

The enthalpy change of a sample with the temperature can be related with the heat capacity of the sample at constant pressure, C_p. The heat capacity at constant pressure, C_p, is given by the following equation [25]:

$$C_p(T) = \left(\frac{\partial H}{\partial T} \right)_p \tag{1.1}$$

The heat capacity at constant pressure is used to relate the enthalpy change with the temperature. For infinitesimal changes of temperature, at constant pressure:

$$dH = C_p \cdot dT \tag{1.1}$$

For a short temperature interval the heat capacity could be taken as constant and the enthalpy of a process associated with a the temperature change can be derived from equation 1.3.

$$\Delta H = C_p \cdot \Delta T \tag{1.3}$$

And at constant pressure, related with the heat involved in the process, equation 1.4.

$$q_p = C_p \cdot \Delta T \tag{1.4}$$

The heat capacity can be derived from the balance of the heat transferred to the sample, at constant pressure along the temperature change.

The heat capacity is one of the basic thermophysical and thermodynamic properties that characterizes a compound. In thermochemistry, heat capacity is the amount of energy as heat required to raise the temperature of a sample by one degree [26].

The isobaric heat capacity is required for the calculation of temperature dependence of fundamental thermodynamic functions (some of them were computed in this work as the case of the enthalpy and entropy change). The knowledge of those thermodynamic functions in ILs are important and essential for the understanding of the physical-chemistry properties and behavior of the ILs [27].

1.7.1. Heat capacity measurements

In all measurements, a typical methodology was used. This method consists in the combination of three different measurements to achieve the heat capacity of the sample (the reference cell is measured simultaneously):

1. An empty sample cell measurement (the obtained peak area is A_B);
2. A measurement where the sample cell is filled with the reference material, in this case sapphire (the obtained peak area A_{sapp}), with known heat capacity ($C_{(p,sapp)}$);
3. And a final measurement where the sample cell is filled with the sample (the obtained peak area - A_s).

A graphical representation can be seen in Figure 1.7.
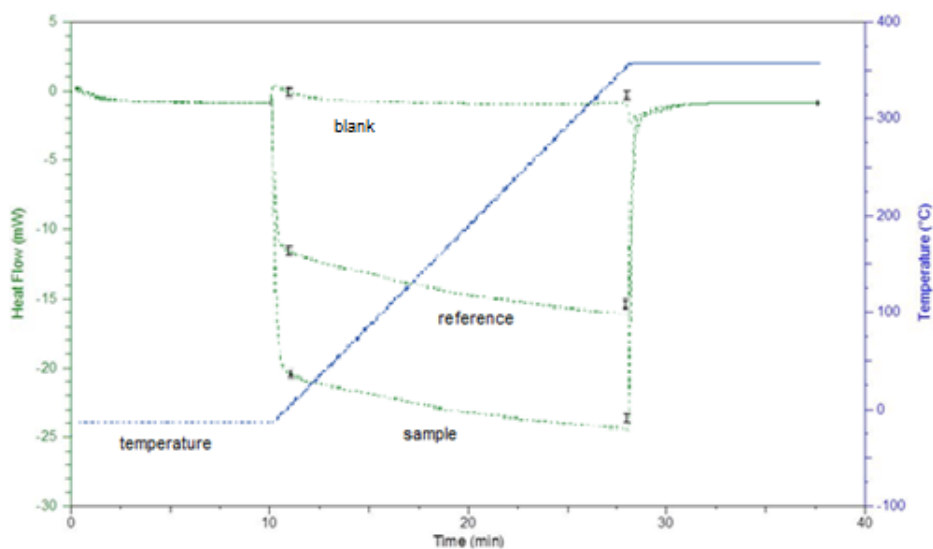
Figure 1.7 - Graphical representation of the three-step method used in the measurements.

Most of the images presented in the figures were taken from print shots of the data analysis software and the temperature labelling is presented in Celsius (ºC). Along the thesis text the temperature, T is presented and discussed in Kelvin (K). The experimental temperature data was converted to Kelvins (K) by the following equation:

$$T(K) = 273.15 + T(°C) \qquad (1.5)$$

The experimental heat capacity measurements were done following two different methodologies: step method and continuous method:

- **Step method** - the temperature of the sample is programmed in step mode with 5 K "jumps" at 0.3 K·min^{-1} (before and after the temperature jump, the temperature keep in isothermal mode for 2600 s);
- **Continuous method** - the temperature of the sample is programmed to change continuous with a fixed temperature scanning rate of 0.3 K·min^{-1} along all the measuring temperature interval.

Figure 1.8 and Figure 1.9 presents a schematic representation of the two methodologies: step method and continuous method, respectively.
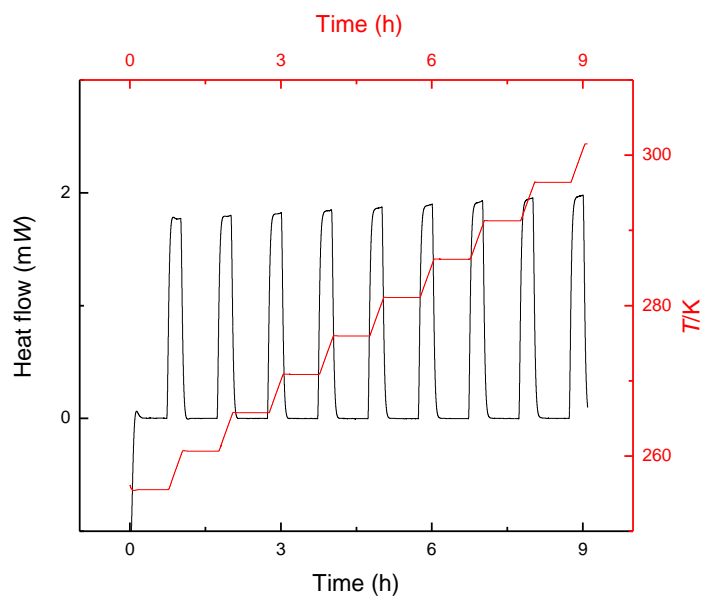
Figure 1.8 – Schematic representation of the temperature program and heat flow in the step method (each temperature jump is 5 K at 0.3 K·min^{-1}, between two temperature stabilizations of 2600 s).
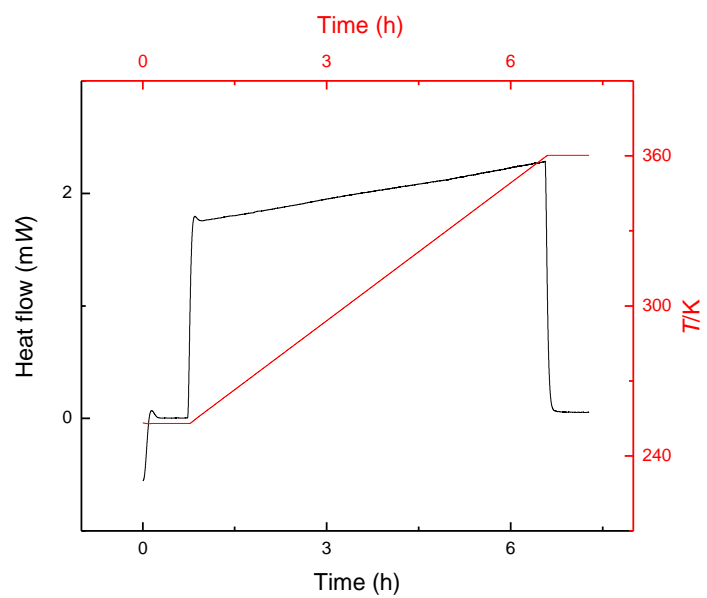
Figure 1.9 – Schematic representation of the temperature program and heat flow in the continuous method (0.3 K·min^{-1}).

1.7.2. Step method

The Step method heat capacity measurement were performed with a sample and reference (an empty pan) simultaneously, being the final results the difference between the sample and the reference, related with the sample heat capacity. The temperature steps are scanned over the experimental temperature range.
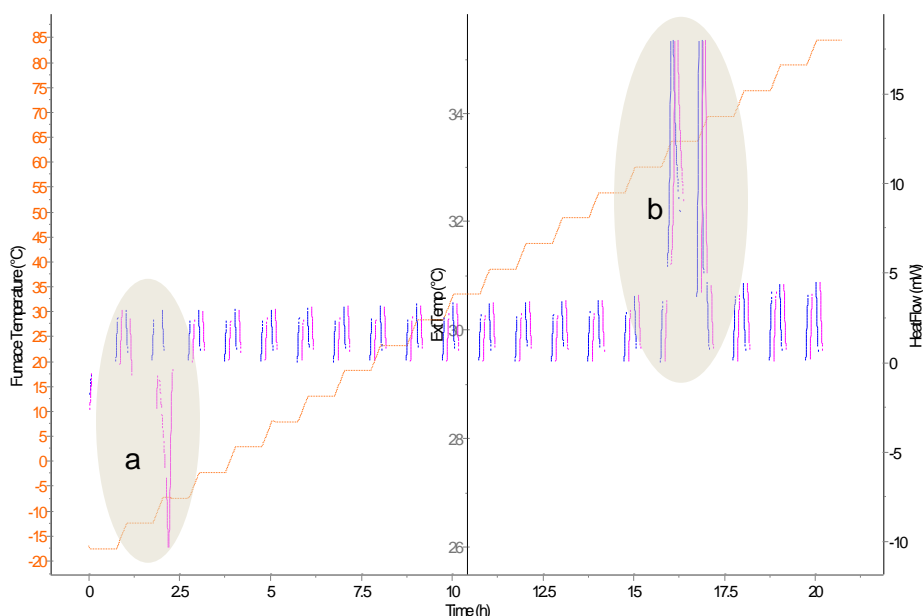
Figure 1.10 - Typical DSC obtained from μDSC IIIa with step method. (e.g. [Bnmim] [BF$_4$] at 0.3 K·min^{-1} in the temperature range of 273 to 355 K).

In Figure 1.10, a typical result for the step method heat capacity measurement is presented. The 1st run is depicted and the blue line; the 2nd run (step sequence of heating) heat capacity measurement is present as the pink line; the calorimeter temperature profile is depicted as the red dash line. In the 1st run the temperature and heat of melting is depicted (*b* zone of figure 1.10). In the 2nd run and due to the fast cooling of the sample, the cool crystallization peak can be detected (in the zone *a*, the pink line).

In the Step method, the heat capacity, at a given temperature, *T* (average temperature of the step temperature interval), was derived by eq.1.6 [21, 23].

$$C_{p,s}(T) = \frac{m_{sapp} \cdot C_{p,sapp}(T) \cdot \dfrac{\left(A_s - A_B\right)}{\Delta T}}{m_s \cdot \dfrac{\left(A_{sapp} - A_B\right)}{\Delta T}} \qquad (1.6)$$

Where $C_{p,s}$ is the sample heat capacity at constant pressure, $C_{p,sapp}$ is the sapphire heat capacity at constant pressure, m_{sapp} is sapphire mass, m_s is sample mass, A_s is the sample peak area, A_B is the blank peak area, A_{sapp} is the sapphire peak area, ΔT is the peak temperature interval (ΔT is the difference between the T_f and T_i for each one of the steps, approximately 5 K)

The step temperature methodology is generally considered more reliable and accurate than the continuous scanning methodology, due to the improved thermal equilibrium attained in the step methodology. The continuous scanning methodology presents the advantage of a continuous temperature scanning that could indicate and detect small heat capacity changes in the sample in the working temperature interval.

1.7.3. Continuous method

This procedure consists in increasing temperature at constant rate. For this work this method was performed with reference (an empty pan) simultaneously, in identical experimental conditions, being the observed results (in Figure 1.11) the difference between the sample and the reference and, so, directly proportional to the sample heat capacity.
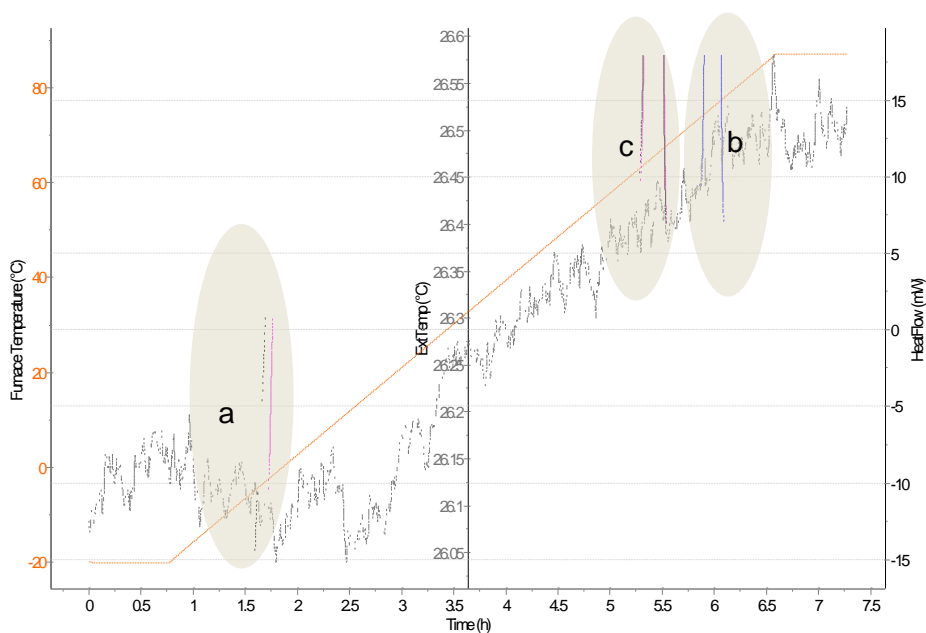
Figure 1.11 - Typical DSC picture from μDSC IIIa with continuous method. Measurement was performed for [Bnmim] [BF$_4$] at 0.3 K·min^{-1} in the temperature range of 273 to 355 K.

In blue is represented the 1st heat flow measurement (the sample is totally crystallized and no cold crystallization is observed in *a* zone), in pink and in black the second measurement and the third measurement respectively (due to the sample fast cooling, the crystallization can be seen in *a* zone). In red dash the calorimeter temperature. It can be seen that there is only the fusion effect in the first measurement (*b* zone), due to thermal history of the sample. Due to the initial crystal phase being different of the crystal phase obtained for the second and third measurement, the melting peak occurs at lower temperature (zone *c*) than the first measurement.

In the continuous methodology, the heat capacity, at a given temperature, T was derived using eq.1.7 :

$$C_{p,c}(T) = \frac{m_{sapp} \cdot C_{p,sapp}(T) \cdot \left(\dfrac{\phi_s}{\beta} - \dfrac{\phi_B}{\beta} \right)}{m_s \cdot \left(\dfrac{\phi_{sapp}}{\beta} - \dfrac{\phi_B}{\beta} \right)} \qquad (1.7)$$

Where $C_{p,s}$ (T) is the sample heat capacity at constant pressure, $C_{p,sapp}$ (T) is the sapphire heat capacity at constant pressure, m_{sapp} is sapphire mass, m_s is sample mass, ϕ_s is the sample heat flow, ϕ_B is the blank heat flow, ϕ_{sapp} is the sapphire heat flow and β is the average heating (0.3 K·min^{-1}) that shall be very similar for each one (sapphire, sample and blank).

1.8. Phase Transitions measurements

1.8.1. Introduction to phase transition studies

All known substances have different homogeneous states resulting of different molecular arrangements that leads to different properties, allowing the phase distinguishing. Those molecular arrangements in a single substance are known as phase transitions. Phase transitions can be observed in thermal analysis techniques and their different behaviours can be divided into first-order transitions and second order transitions [28]:

- **First-order transitions** – are accompanied by discontinuities of thermodynamic quantities such as entropy and density (glass transition, cold crystallization, melting);
- **Second-order transitions** – for which the thermodynamic potentials and their first-order derivatives are continuous, while some second derivatives with respect to state variables are reduced to zero or approach infinite asymptotically at the transition point.

In this work first-order transitions will be studied in the ILs, such as glass transition, cold crystallization, solid-solid transitions and melting. The solidification of a liquid in the form of a glass, is the glass transition and can be observed as a change in the heat flow value (in figure 1.12, region *a*) – the ΔC_p.

The cold crystallization occurs when there is a formation of solid crystals, from a primary liquid phase (when cooling the sample), through two processes: nucleation and nuclei growth. It can be observed as then an exothermic peak in the heat flow of figure 1.12 (region *b*).

The melting temperature is the temperature at which, under a specified pressure, the liquid and solid phase boundaries meet and all three phases are in mutual equilibrium. This can be observed in figure 1.12 as an endothermic peak (region *c*).

The different peak sizes are due to different heating\cooling temperature rates. In the first measurement, a higher heating rate leads to a thinner and longer peak when compared with the second measurement with a lower cooling rate.
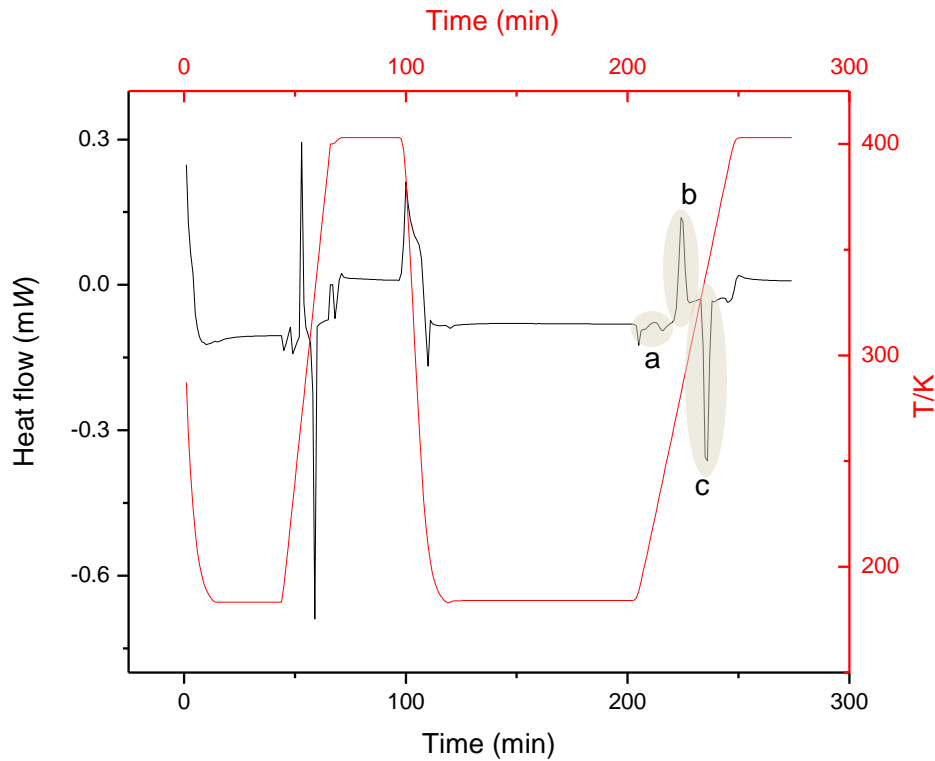
Figure 1.12 - Results obtained in TA Q1000 for [Bnmim] [BF$_4$], the first run was performed at 5 K·min^{-1}, and the second one was performed at 3 K·min^{-1}. Both measurements occurred in the temperature range of 183 to 423 K.

When a phase transition is detected a procedure must be taken into account, so all phase transition temperatures can be identified in a rigorous way: the onset temperature (T_{onset}). So, in this work, the temperatures of the phase transitions of the studied compounds were taken as the onset temperature:

- Glass transition temperature, T_g is the midpoint of a small heat capacity change on heating from the amorphous glass state to a liquid state;

- Cold crystallization temperature, T_{cc} is the onset of an exothermic peak on heating from a subcooled liquid state to a crystalline solid state;

- Melting point, T_m was considered as the onset of an endothermic peak of melting on heating.

1.8.2. Crystallization

Crystallization occurs when there is a formation of solid crystals, from a primary liquid phase (when cooling the sample), through two processes:

- Nucleation;
- Nuclei growth.

Other form of crystallization occurs when the sample is slowly heated above the T_g, forming crystalline structures – the cold crystallization, T_{cc} [29]. Both processes occur from a less organized structure, amorphous liquid or solid, to a more organized or crystalline structure. An amorphous solid state is characterized by a not totally crystallized compound where some molecules have freedom to move, explaining the rubbery state that characterizes this phase. This is presented in the thermogram as multiple melting or crystallization peaks, what means that such samples are difficult to crystallize in one step and, in a general way, those compounds possess long alkyl side chains that tend to crystallize in steps, due to C-C (carbon-carbon) bond rotation. These solid-solid phase transitions occurring before the melting point are often referred to as rotator phases, which generally possess plastic properties [30]. These need even longer cooling so that one-step crystallization can be reached as seen in Figure 1.13.
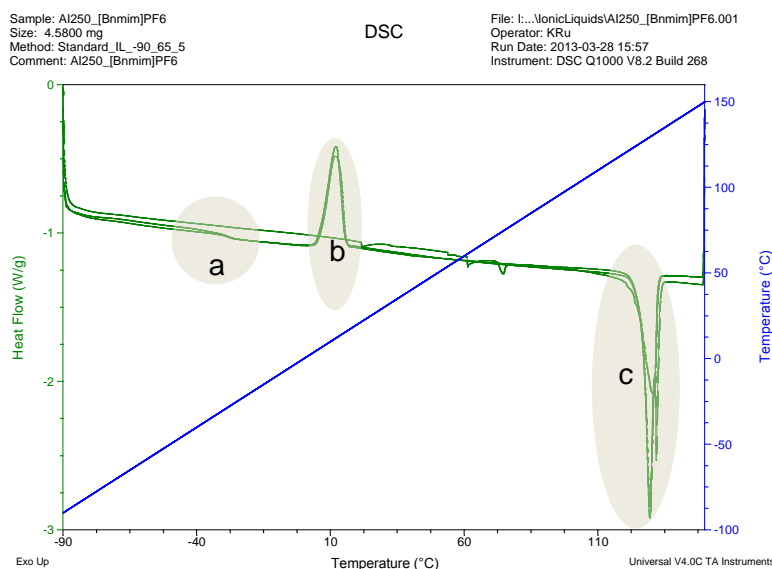
Figure 1.13 - In this example, different peaks can be seen, along the sample heating. All were performed under the same experimental conditions, in the temperature range of 183 to 423 K, at 5 K·min^{-1}. *a*, *b* and *c* are the glass transition, the cold crystallization and the melting peak, respectively.

Those different peaks size are due to different crystallization degrees, this is proved by the fact of not having a cold crystallization peak in the first measurement and different peak sizes in the following measurements. In the first measurement, since the compound is totally crystalline, the heat flow is higher and there is no cold crystallization peak. In the second measurement, due to a fast cooling, some of the sample didn't have time to crystallize and so there is a lower heat flow signal (so, a lower heat capacity) and a first, smaller cold crystallization peak, from the amorphous crystal part. In the last measurement, the sample is totally in an amorphous state and so, the heat flow is represented by the lower heat flow signal and the higher crystallization peak.

The use of a fast cooling rate can show amorphous areas in samples and slow cooling leads to higher degrees of crystallization. This can be better seen in Figure 1.14.
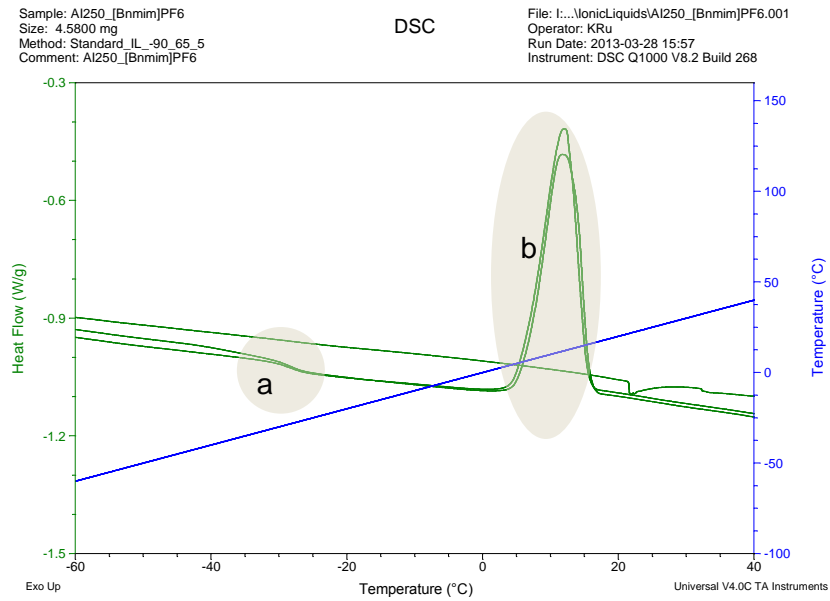
Figure 1.14 – Example of different crystallization degrees in ILs, performed for the same sample, under the same experimental conditions, in the temperature range of 183 to 423 K, at 5 K·min⁻¹. *a*, and *b* are the glass transition and the cold respectively.

1.8.3. Glass transition

A glass transition or the liquid-glass transition, T_g, is the reversible transition in amorphous materials from a molten or rubberlike state into a hard and relatively brittle state and vice-versa [31].

This is an important characteristic, considering that some ILs only show a crystallization peak – cold crystallization - after heating from low temperatures. Usually, the cold crystallization peak can be seen from 20 to 30 temperature degrees after the glass transition. Also, some ILs do not present crystallization peak, until the glass transition temperature is achieved, staying in a supercooled liquid state [32]. In the previous cases, the transition kinetics, mainly governed by the cooling rate (rapid or slow cooling), plays an important role, so, in order to obtain reliable thermal phase behavior data, long equilibration times and small samples are needed.

Usually, the T_g can be difficult to determine because it can take place over a wide temperature range and is highly dependent on conditions such as the measurement method and pressure [33]. For 1-alkyl- 3-methylimidazolium salts, T_g recorded are typically in the region between 203 K and 183 K [34].

The T_g can also be related with the sample melting temperature as shown in eq. 1.8 (temperature values are presented in K) [35]:

$$T_g/T_m \text{ (K)} = 2/3 \tag{1.8}$$

And for most of the studied ILs:

$$T_g/T_m \text{ (K)} = [2/3; 3/4] \tag{1.9}$$

1.8.4. Melting point

Melting point is the temperature which, at atmospheric pressure, there is a phase transition from solid to liquid state. Typically, at this temperature, the sample is in solid-liquid equilibrium and remains isothermal, until the whole sample is melted.[36]

In the ILs, the melting point is deeply influenced by many factors [37]:

- different cation and anion size can lead to a lower fusion temperature (weaker electrostatic interactions in the crystal lattice);
- symmetrical ions leads to higher fusion temperatures (better crystal packing);
- great charge delocalization leading to lower fusion temperature.

1.9. Group contribution methods

Nowadays, the number of known ILs is around thousands (and their number is still growing!) and so, to analyse all of them not feasible. In addition, some properties such as T_g, cannot be measured due to apparatus limitations regarding for example working temperature range. To solve this kind of problems, the prediction methods are developed and used to obtain missing data.

The most used prediction methods are those based on a group contribution concept, where the group is defined as a set of atoms with a well-defined value for a given property. From the established contributions, one can calculate the physicochemical properties of a compound of interest (if all contributions, to which the compound is divided, are available).

For example, the glass transition temperature can be estimated from the following groups sum (eq.1.10) [34]:

$$T_g = \Sigma \ contribution \ of \ composing \ groups \ + \ \Sigma \ corrections \ where \ necessary \quad (1.10)$$

Where all the groups contribute for the first equation portion plus some corrections necessary, previously determined through studies (as well as all the values defined for each group and respective corrections).

1.9.1. Group contribution method for heat capacities

For heat capacities an estimation method used by Gardas *et al* [27] is presented in equation 1.11.:

$$C_p(T/K) = R\left[A + B\left(\frac{T}{100}\right) + D\left(\frac{T}{100}\right)^2\right]$$

(1.11)

where R is the gas constant (R=8.314462 J·K^{-1}·mol^{-1}), T is the absolute temperature in K, and A, B and D are constants obtained from the following relations (eq: 1.12; 1.13 and 1.14):

$$A = \sum_{i=1}^{k} n_i a_i$$

(1.12)

$$B = \sum_{i=1}^{k} n_i b_i$$

(1.13)

$$D = \sum_{i=1}^{k} n_i d_i$$

(1.14)

Where n is the number of times that the i group appears, and a, b and d are fitted parameters [27].

1.9.2. Group contribution method for phase transitions

For ionic liquids, phase transition temperatures can be predicted through the equation 1.15, due to the effect of the pair anion/cation as suggested by Lazzús [34]:

$$T_g = C + n_i \Delta t_{ci} + n_j \Delta t_{aj}, \tag{1.15}$$

where T_g (K) is the temperature of glass transition, C is a constant, n_i and n_j are the number of times that the groups i and j appear in the compound, Δt_{ci} is the cation contribution and Δt_{aj} is the anion contribution for the molecule. An identical equation was used for melting temperatures in the GCM.

2. Experimental part

2.1. Ionic liquids description

Some of the ionic liquids under study are viscous liquids (transparent to yellow colour), other are solids (white powder) with molecular weights between 250 and 450 g mol^{-1} (the relative atomic masses used were those recommended by the IUPAC Commission in 2007 [38]). All of the ionic liquids were purchased from IOLITEC with a stated purity of better than 99%, which is the necessary for this kind of studies.

2.1.1. 1-Benzyl-3-methylimidazolium ([Bnmim]$^+$) based ILs

The first group consists of four ILs (Table 2.1) with a common cation – the 1-benzyl-3-methylimidazolium, and four different anions which displays different characteristics between them (volume, charge dispersion, cation interaction): the BF$_4$, the PF$_6$ (these two are amply investigated nowadays), the NTf$_2$ and the C$_2$F$_4$HSO$_3$ (these last two are recent and more is needed to discover about them. The information regarding this ionic liquid family is compiled in Table 2.1.

Table 2.1 – Summary of the 1-Benzyl-3-methylimidazolium [Bnmim]$^+$, based ionic liquids.

Compound name	Abbreviation	CAS number	Supplier/ Purity	Molecular weight (g/mol)	Compound visual aspect
1-Benzyl-3-methylimidazolium tetrafluoroborate	[Bnmim] [BF$_4$]	500996-04-3	IoLiTec/ >99%	260.04	White powder
1-Benzyl-3-methylimidazolium hexafluorophosphate	[Bnmim] [PF$_6$]	433337-11-2	IoLiTec/ >99%	318.20	White powder
1-Benzyl-3-methylimidazolium 1,1,2,2-tetrafluoroethanesulfonate	[Bnmim] [C$_2$F$_4$HSO$_3$]	n/a	IoLiTec/ >99%	354.32	Amorphous white solid
1-Benzyl-3-methylimidazolium bis(trifluoromethylsulfonyl)imide	[Bnmim] [NTf$_2$]	433337-24-7	IoLiTec/ >99%	453.38	Yellow viscous liquid

2.1.2. 1-Alkyl-3-methylimidazolium hexafluorophosphate ($[C_nC_1im][PF_6]$) based ILs

In Table 2.2, the second group of the studied ILs is presented. It consists of ten ILs, each one with different alkyl chain lengths as mentioned before: -methyl, -ethyl, -propyl, -butyl, -pentyl, -hexyl. –heptyl, -octyl, -nonyl, -decyl and -dodecyl-3-methylimidazolium hexafluorophosphate. This group was chosen to study the alkyl chain size effect on the studied properties. The analysis and the rationalization of the obtained results will be done considering the literature data for the $[C_{N-1}C_1im][NTf_2]$[39].

Table 2.2 - Summary of the 1-alkyl-3-methylimidazolium hexafluorophosphate, $[C_nC_1im][PF_6]$, ionic liquids series

Compound name	Abbreviation	CAS number	Supplier/ Purity	Molecular weight (g/mol)	Compound visual aspect
1-Ethyl-3-methylimidazolium hexafluorophosphate	$[C_2C_1im][PF_6]$	155371-19-0	IoLiTec/ >99%	256.06	White crystals
1-Propyl-3-methylimidazolium hexafluorophosphate	$[C_3C_1im][PF_6]$	216300-12-8	IoLiTec/ >99%	270.07	White crystals
1-Butyl-3-methylimidazolium hexafluorophosphate	$[C_4C_1im][PF_6]$	174501-64-5	IoLiTec/ >99%	284.08	Light yellowed viscous liquid
1-Pentyl-3-methylimidazolium hexafluorophosphate	$[C_5C_1im][PF_6]$	280779-52-4	IoLiTec/ >99%	298.09	Yellowed viscous liquid
1-Hexyl-3-methylimidazolium hexafluorophosphate	$[C_6C_1im][PF_6]$	304680-35-1	IoLiTec/ >99%	312.10	Yellowed viscous liquid
1-Heptyl-3-methylimidazolium hexafluorophosphate	$[C_7C_1im][PF_6]$	357915-04-9	IoLiTec/ >99%	326.11	Yellowed viscous liquid
1-Octyl-3-methylimidazolium hexafluorophosphate	$[C_8C_1im][PF_6]$	304680-36-2	IoLiTec/ >99%	340.12	Yellowed viscous liquid
1-Nonyl-3-methylimidazolium hexafluorophosphate	$[C_9C_1im][PF_6]$	n/a	IoLiTec/ >99%	354.13	Darker yellowed viscous liquid
1-Decyl-3-methylimidazolium hexafluorophosphate	$[C_{10}C_1im][PF_6]$	n/a	IoLiTec/ >99%	368.14	White/orange crystals
1-Dodecyl-3-methylimidazolium hexafluorophosphate	$[C_{12}C_1im][PF_6]$	219947-93-0	IoLiTec/ >98%	394.16	White/orange crystals

2.2. Drying procedure

Impurities, such as water, are likely to produce great uncertainty in the phase transitions and at heat capacities measurements. Therefore, all the samples were dried during one week, without heating, to avoid the samples degradation. They were kept under low pressure, in the presence of a cold trap at 228 K, to remove water and other possible contaminants.

The drying system is shown in Figure 2.2, and basically consists a vacuum pump system (marked as 5 in Figure 2.1)and its three basic components:

- Edwards RV3 rotary vacuum pump;
- Pfeiffer Balzers TCP 310 turbo pump controller;
- Pfeiffer Balzers TPU-170 turbomolecular vacuum pump.
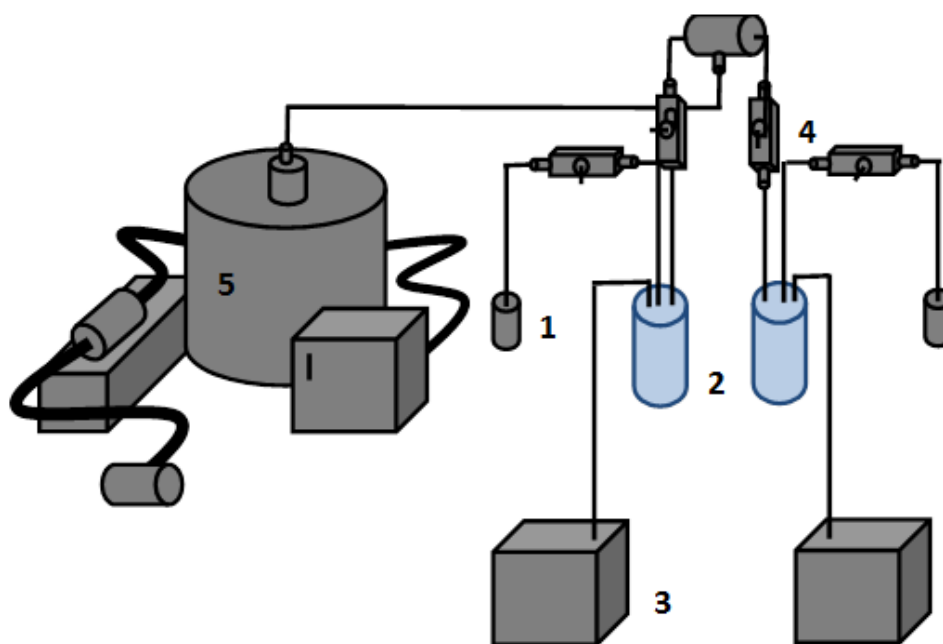
Figure 2.1 - Scheme of the drying system: 1- Sample vessel; 2- Cold trap (glass); 3- Cooling system; 4- Valves; 5- Vacuum pump system.
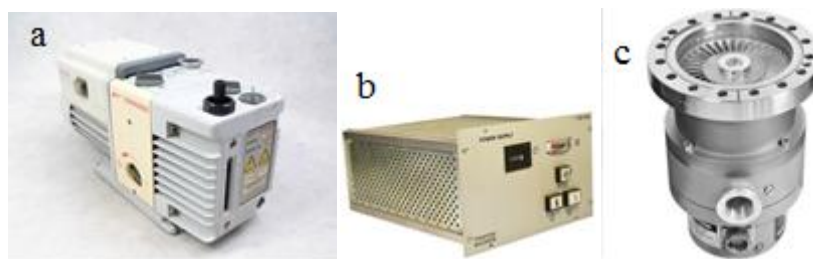
Figure 2.2 - Components of the vacuum system: a- Edwards RV3 rotary vacuum pump; b- Pfeiffer Balzers TCP 310 turbo pump
controller; c- Pfeiffer Balzers TPU-170 turbomolecular vacuum pump.

The results describing the drying process are presented in Table 2.3.

Table 2.3 - Initial mass (before drying), final mass (after drying) and mass loss for the studied ionic liquids.

Compound	Initial m_{sample} (g)	Final m_{sample} (g)	Mass loss (g)	% Mass loss
[Bnmim][BF$_4$]	1.85	1.85	0.00	0.0
[Bnmim][PF$_6$]	0.41	0.40	0.01	2.5
[Bnmim][NTf$_2$]	1.20	1.20	0.00	0.0
[Bnmim][C$_2$F$_4$HSO$_3$]	1.86	1.86	0.00	0.0
-	-	-	-	-
[C$_2$C$_1$im][PF$_6$]	1.00	0.98	0.02	2.0
[C$_3$C$_1$im][PF$_6$]	1.04	1.03	0.01	1.0
[C$_4$C$_1$im][PF$_6$]	0.87	0.87	0.00	0.0
[C$_5$C$_1$im][PF$_6$]	2.06	2.06	0.00	0.0
[C$_6$C$_1$im][PF$_6$]	1.94	1.94	0.00	0.0
[C$_7$C$_1$im][PF$_6$]	1.40	1.40	0.00	0.0
[C$_8$C$_1$im][PF$_6$]	1.74	1.64	0.10	6.1
[C$_9$C$_1$im][PF$_6$]	2.08	2.08	0.00	0.0
[C$_{10}$C$_1$im][PF$_6$]	1.11	1.10	0.01	0.9
[C$_{12}$C$_1$im][PF$_6$]	1.05	1.04	0.01	1.0

2.3. Calorimeters calibration

2.3.1. Enthalpy and temperature calibration

For the temperature and enthalpy calibration, five substances had been selected (water, gallium, naphthalene, indium and tin). High purity naphthalene, tin and indium were purchased from the German Society of Thermal Analysis (GEFT) and are part of the selection, which is called "Calibration Substances for Heat and Temperature Calibration of Differential Scanning Calorimeters". Gallium was provided from the Research Institute of Metals with a purity of 99.9999%. Water (Milipore quality) was prepared at the Institute of Physical Chemistry, an Institute of Chemical Technology Prague device, using Millipore Milli-QRG. Anthracene was purchased from Sigma-Aldrich with a stated purity of 99.5%. The measurements were performed in the same vessels described before.

Temperature calibration was performed with melting temperature determinations. For the melting point determination, it should be noted that tabulated values only apply to chemically pure substances. In the presence of impurities or additives, the measured temperature is lower than the melting temperature of a pure substance. Measurement is performed, under a constant temperature raise, from approximately 60° below the expected melting temperature (because the substance can act as a subcooled liquid) until a temperature of 20° above the expected melting point. Melting was evaluated as mentioned before.

The vessels used were the same as mentioned earlier.

2.3.2. Calorimeters Stabilization

The calorimeter stabilization is used to refine the measurements reproducibility. In order to evaluate the working stability of the calorimeter system, the stabilization was carried out in the full temperature range, with the respective vessels.

The following compounds were selected based on their availability and literature recommendations. Synthetic sapphire (α-Al_2O_3) derived from two sources: sapphire disks supplied by the manufacturer for the calorimeter calibration; sapphire powder was obtained by grinding the calorimetric standard (NIST Standard Reference Material no. 720).

Since both calorimeters work with small weight samples, it was necessary to ensure the most accurate sample weighing. To do this in a laboratory scale, a Denver Instrument was used, capable of measuring to the nearest hundredth of a milligram. Scales are calibrated periodically by a professional service.

3. Results and discussion

3.1. Phase transitions

The phase behavior was investigated from 183 to 423 K with a differential scanning calorimeter (TA Q1000, TA Instruments, USA) using the continuous method with a heating rate of 5 K·min^{-1}. Samples of about 0.1 g of each ionic liquid were placed in the crucibles and weighted by an analytical balance with a readability of 0.01 mg. After the measurements, the obtained data was analyzed using the TA Universal Analysis software as can be observed in Figure 3.1 and Figure 3.2.
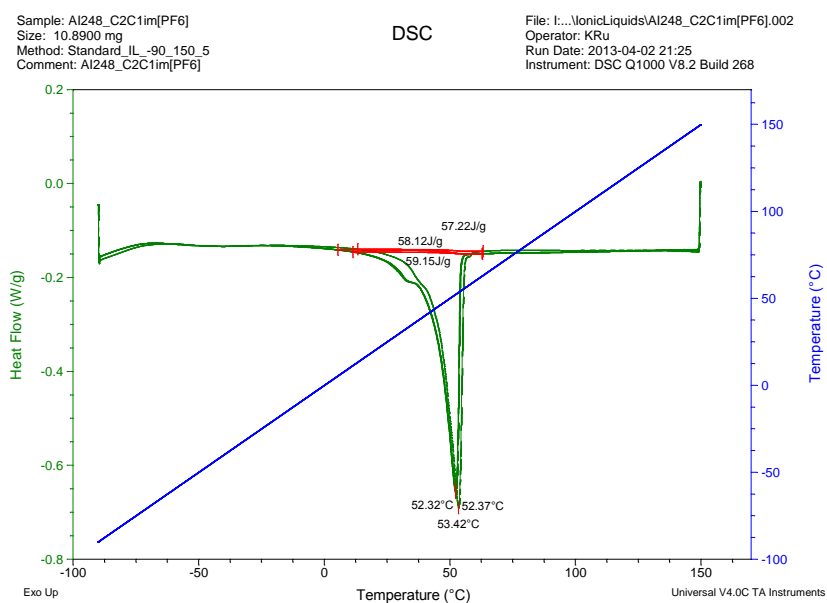
Figure 3.1 - Example of a sample data analysis using TA Universal Analysis software.
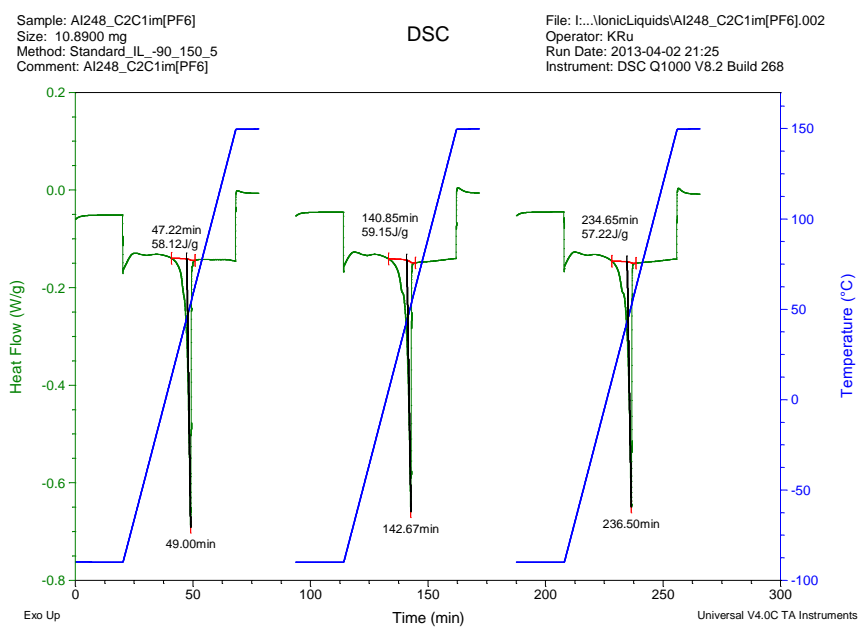
Figure 3.2 - Example of the 3 measurements performed for [C₂C₁im][PF₆] phase transition analysis.

3.1.1. The 1-benzyl-3-methylimidazolium based ionic liquids

The phase transitions results for each compound of the 1-benzyl-3-methylimidazolium series are presented. The thermograms for each compound are presented in figures 3.3 to 3.6.

[Bnmim][BF$_4$] was solid at room temperature and liquid phase was reached at 336 K (62 ºC). Cold crystallization was not observed in the first measurement only appearing in the two following measurements at 282 K (45 ºC). Glass transition was detected at 235 K (-37 ºC). *a* is just an error occurred along the measuring.
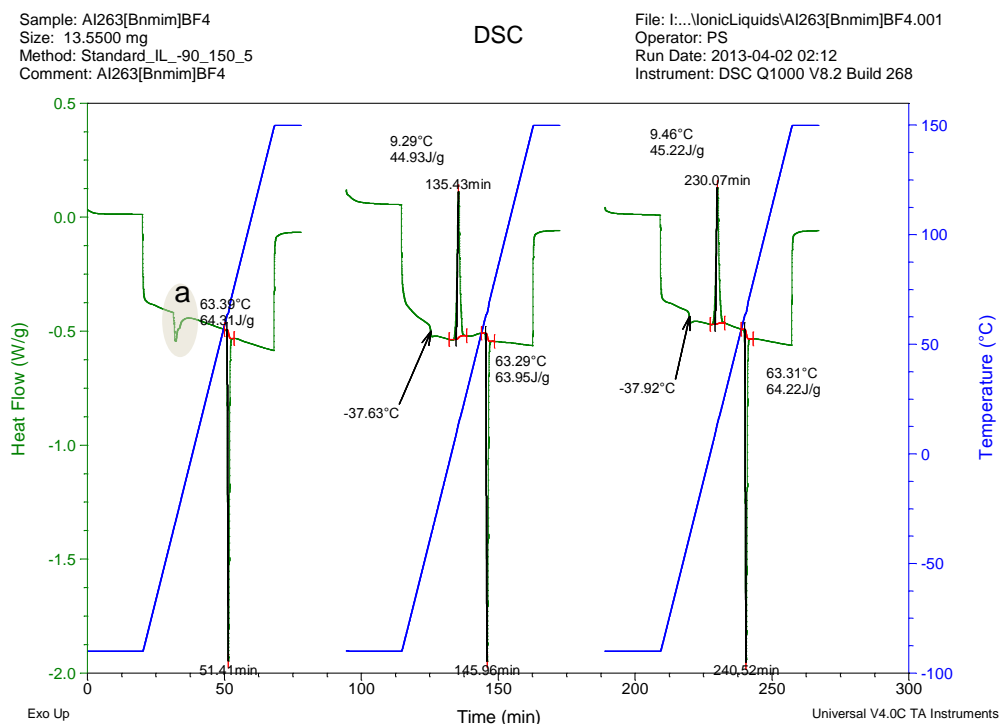
Figure 3.3 - Thermal analysis for [Bnmim][BF$_4$] performed from 183 to 423 K at a 5 K·min^{-1} rate.

[Bnmim][PF$_6$] was solid at room temperature and liquid phase was reached at 399 K (78 ºC). As observed for the previous ionic liquid, the cold crystallization only appeared in the two last measurements at 278 K (5 ºC). Glass transition was detected at 244 K (-28 ºC).
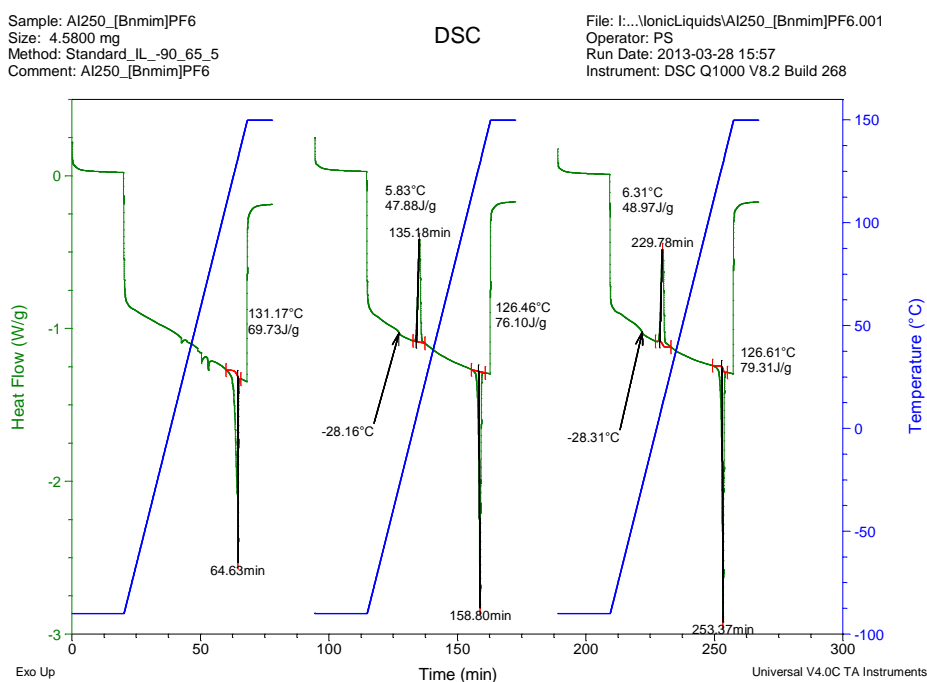
Figure 3.4 - Thermal analysis for [Bnmim][PF$_6$] performed from 183 to 348 K at a 5 K·min^{-1} rate.

The third compound is the [Bnmim][NTf$_2$]. It was liquid at room temperature and solid phase was not reached in the temperature range studied, remaining in a subcooled liquid state until glass transition detection, at 216 K (-57 ºC).
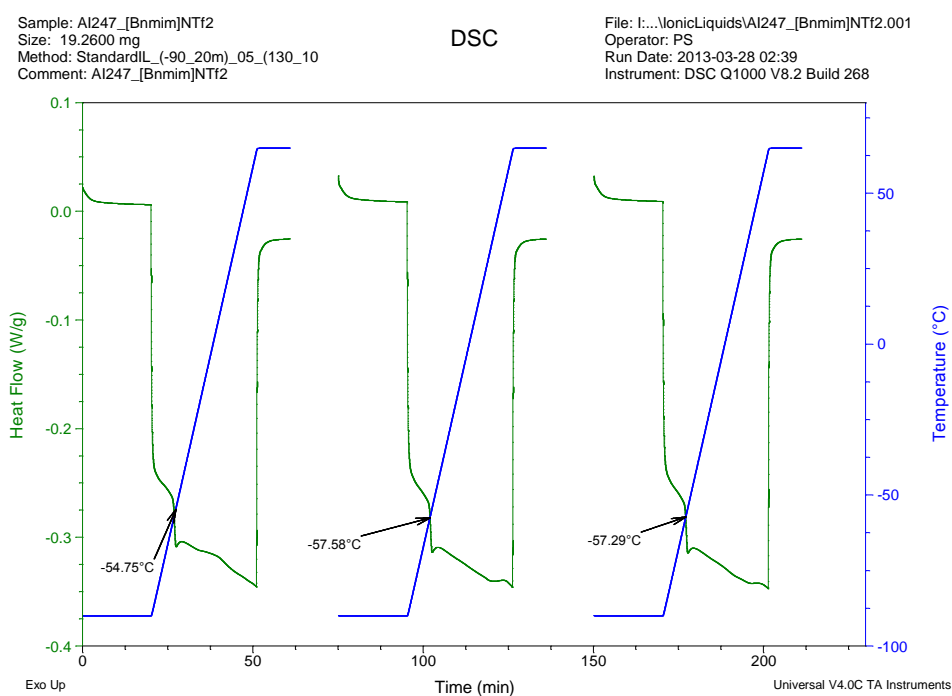
Figure 3.5 - Thermal analysis for [Bnmim][NTf$_2$] performed from 183 to 348 K at a 5 K·min^{-1} rate.

[Bnmim][$C_2F_4HSO_3$] was also solid at room temperature and liquid phase was reached at 315 K (61 ºC). Cold crystallization was not reached in the first measurement appearing in the two measurements after. Glass transition was detected at 229 K (43 ºC), after the first measurement.
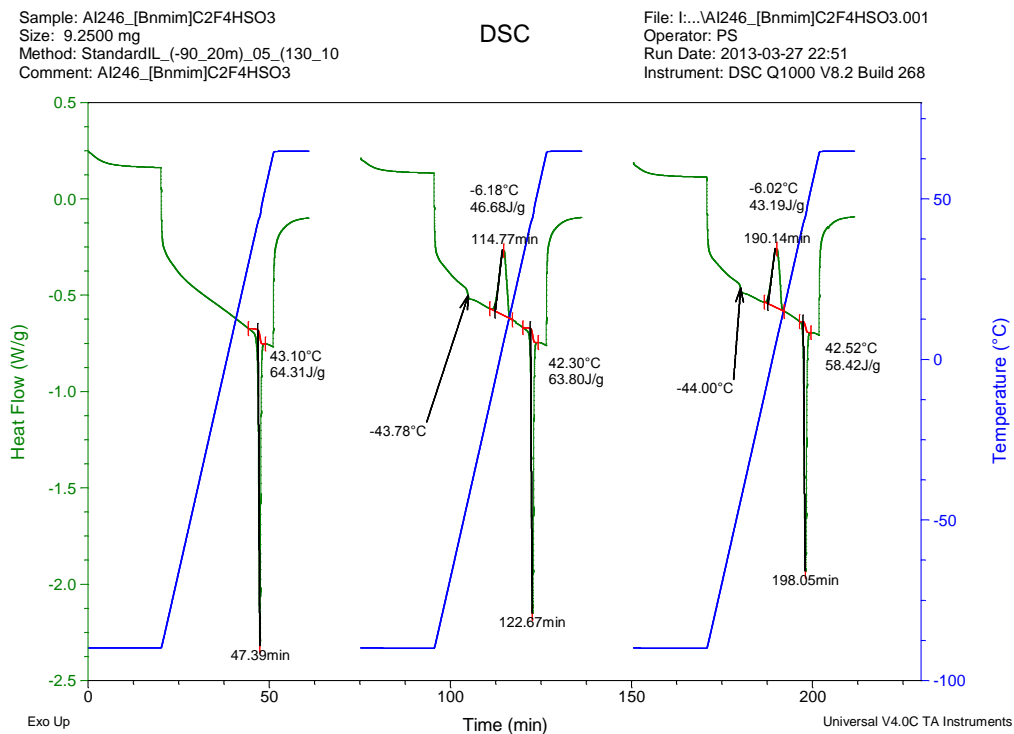
Figure 3.6 - Thermal analysis for [Bnmim][$C_2F_4HSO_3$] performed from 183 to 348 K at a 5 K·min^{-1} rate.

3.1.2. The 1-alkyl-3-methylimidazolium based ionic liquids

The phase transitions results for each compound of the 1-alkyl-3-methylimidazolium series are presented, in the temperature range of 183 K to 423 K (-90 to 150 ºC), at a 5 K·min^{-1} heating rate. The thermograms obtained for this ionicliquids family, $[C_nC_1im][PF_6]$, are presented in figures 3.7 to 3.15.

$[C_2C_1im][PF_6]$ was solid at room temperature and the liquid phase was reached at 317 K (43 ºC). No glass transition or cold crystallization was detected, instead, a solid-solid transition at 232 K (-41 ºC) can be detected.
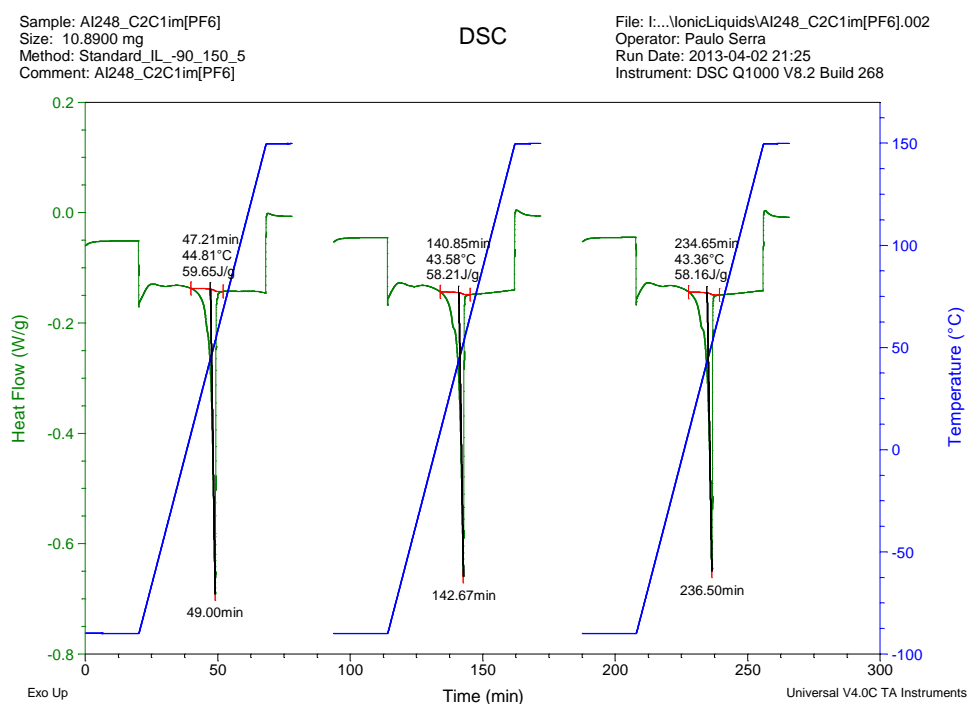
Figure 3.7 - Thermal analysis for $[C_2C_1im][PF_6]$ performed from 183 to 423 K, at a 5 K·min^{-1} rate.

$[C_3C_1im][PF_6]$ was also solid at room temperature and liquid phase was reached at 311 K (38 ºC). Neither the cold crystallization nor the glass transition were observed in the studied temperature range, but a solid-solid transition can be observed at 232 K (-41 ºC).
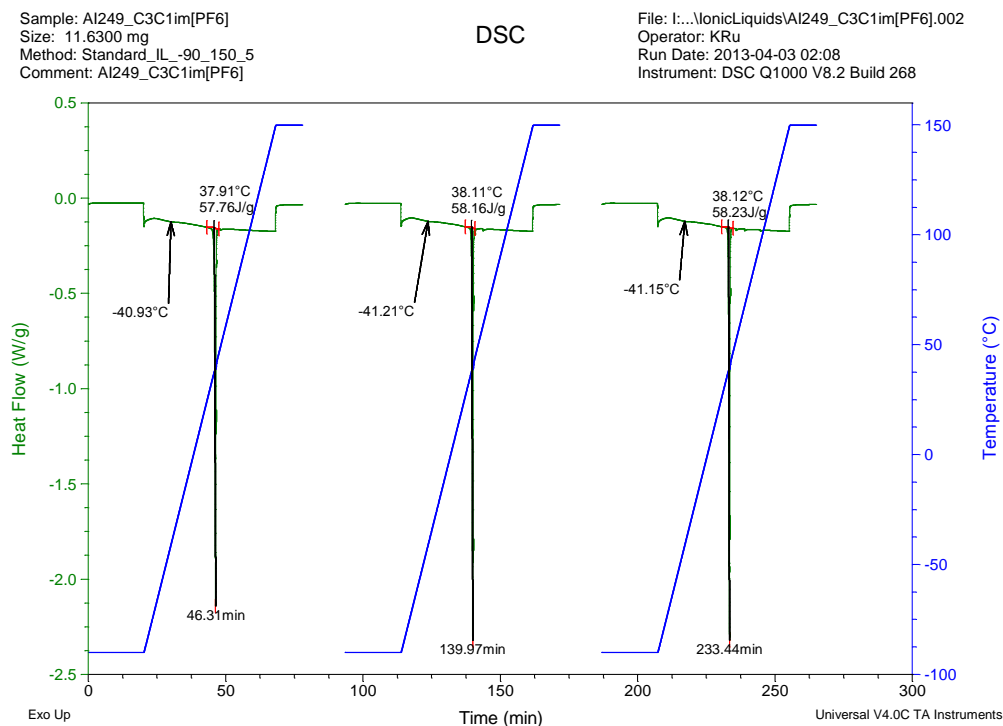
Figure 3.8 - Thermal analysis for [C$_3$C$_1$mim][PF$_6$] performed from 183 to 423 K, at a 5 K·min^{-1} rate.

[C$_4$C$_1$im][PF$_6$] was liquid at room temperature and solid phase was not reached in the measured temperature range. The glass transition was detected at 195 K (-78 ºC).
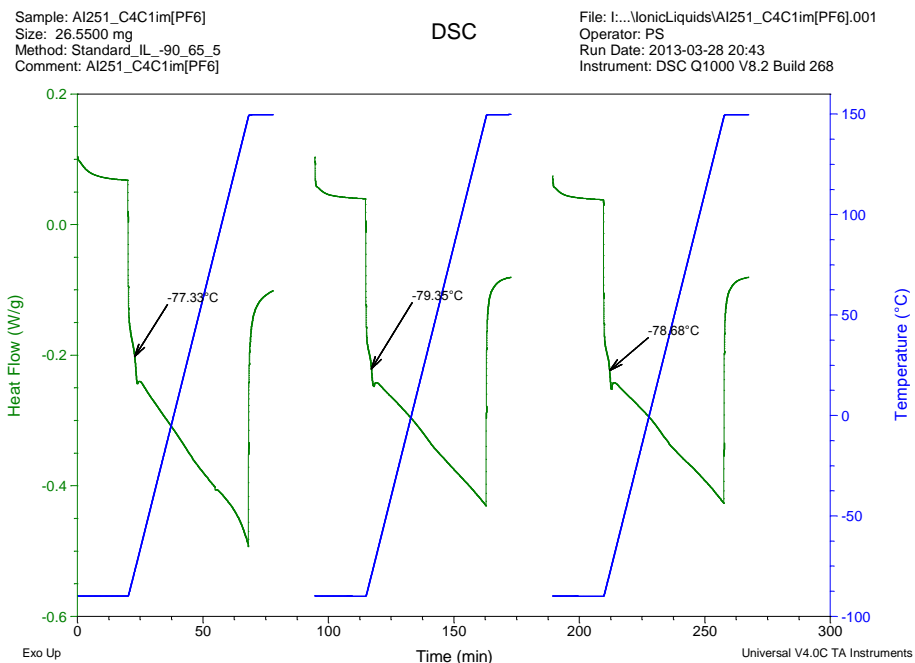
Figure 3.9 - Thermal analysis for [C$_4$C$_1$mim][PF$_6$] performed from 183 to 423 K, at a 5 K·min^{-1} rate.

$[C_5C_1im][PF_6]$ was liquid at room temperature and the solid phase was not reached in the measured temperature range. Glass transition was detected at 199 K (-75 ºC).
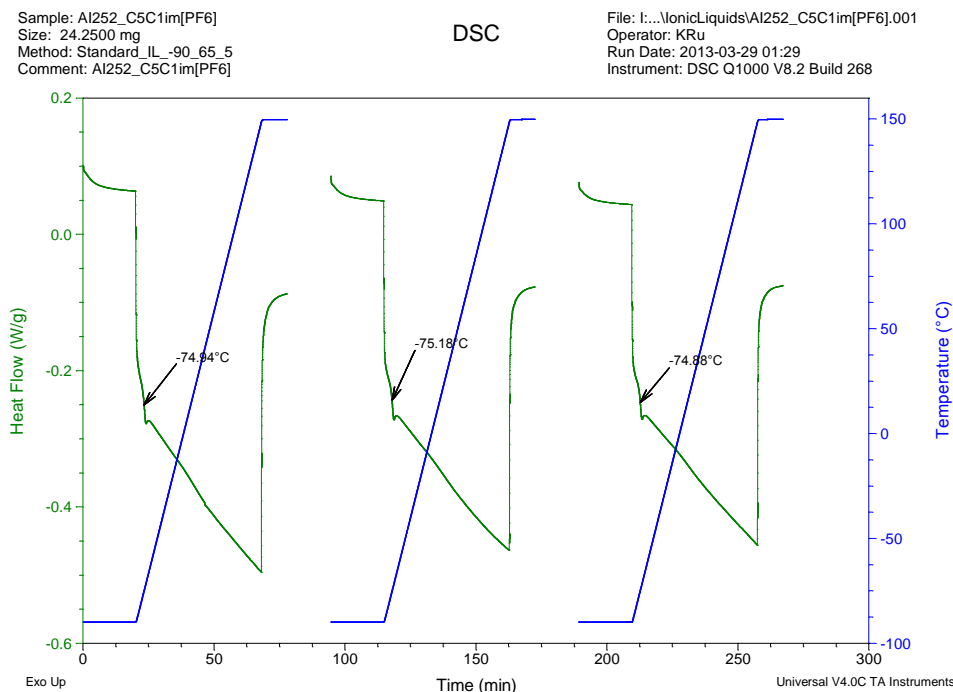
Figure 3.10 - Thermal analysis for $[C_5C_1mim][PF_6]$ performed from 183 to 423 K, at a 5 K·min^{-1} rate.

$[C_6C_1im][PF_6]$ was liquid at room temperature and solid phase was not reached in the measured temperature range. Glass transition was detected at 201 K (-72 ºC).
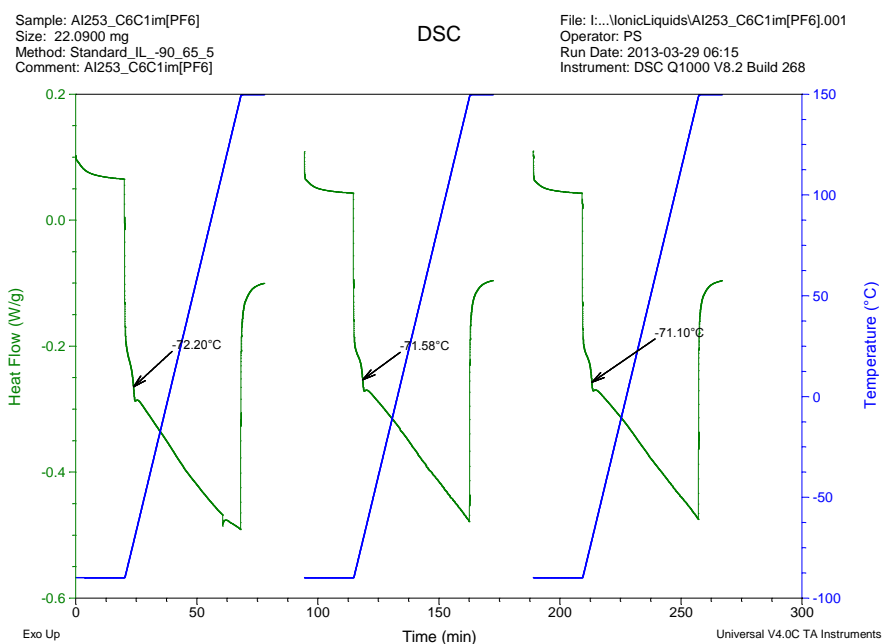
Figure 3.11 - Thermal analysis for $[C_6C_1mim][PF_6]$ performed from 183 to 423 K, at a 5 K·min^{-1} rate.

$[C_7C_1im][PF_6]$ was liquid at room temperature and solid phase was not reached in the measured temperature range. Glass transition was detected at 203 K (-70 ºC).
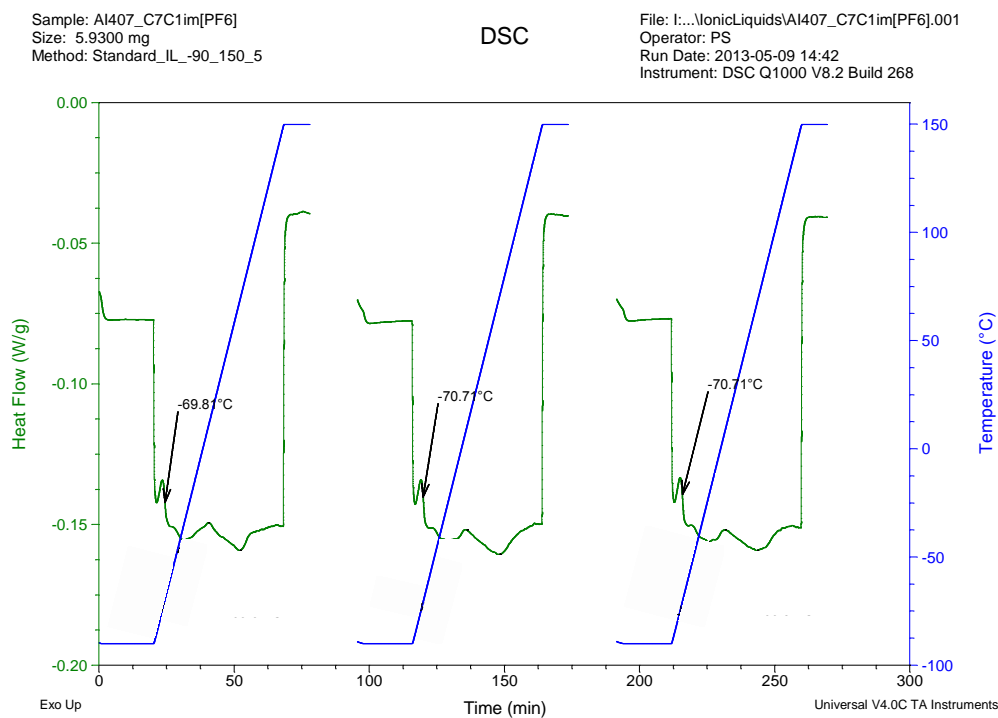
Figure 3.12 - Thermal analysis for $[C_7C_1mim][PF_6]$ performed from 183 to 423 K, at a 5 K·min^{-1} rate.

$[C_8C_1im][PF_6]$ was liquid at room temperature and solid phase was not reached along the studied temperature range. Glass transition was detected at 203 K (-70 ºC). The thermogram of this ionic liquid is not presented due to an occurred error in the data storing.

The following is the $[C_9C_1im][PF_6]$. It was liquid at room temperature before measurements. Was observed the cold crystallization at 252 K (-21 ºC) and the liquid phase was reached at 292 K (19 ºC). Glass transition was detected at 205 K (-67 ºC).
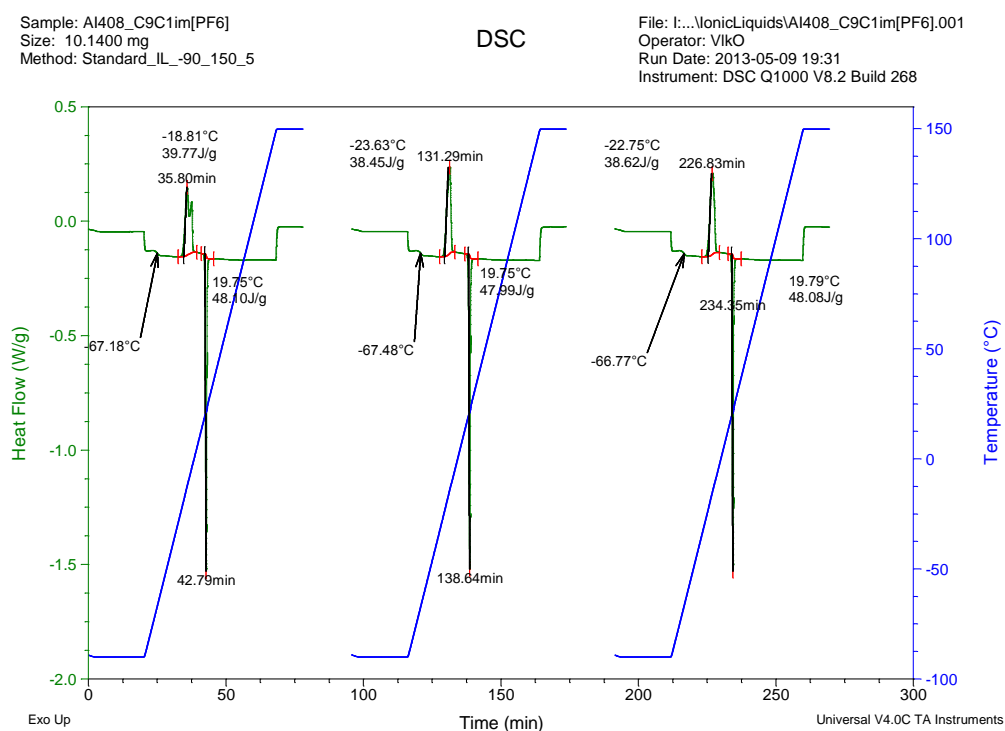
Figure 3.13 - Thermal analysis for $[C_9C_1mim][PF_6]$ performed from 183 to 423 K, at a 5 K·min^{-1} rate.

The following IL is the $[C_{10}C_1im][PF_6]$. It was solid at room temperature and liquid phase was reached in the measured temperature range, at 307 K (34 ºC). Cold crystallization was not reached in the first measurement appearing in the two measurements after. In the first measurement a solid-solid transition at 241 K (-32 ºC)is detected. Glass transition was detected at 208 K (-65 ºC).
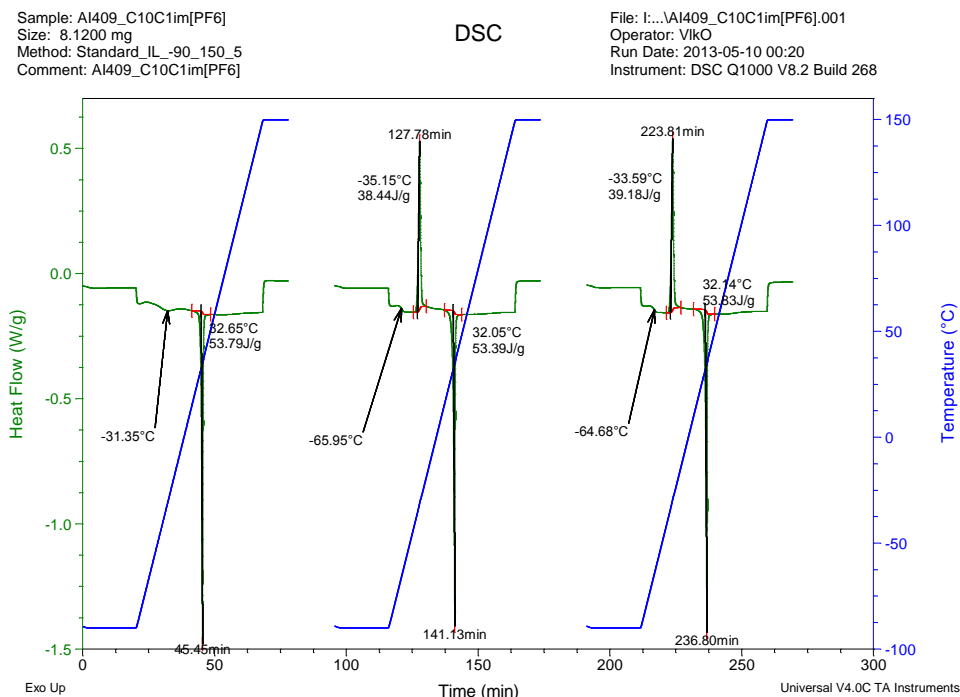
Figure 3.14 - Thermal analysis for [C$_{10}$C$_1$mim][PF$_6$] performed from 183 to 423 K, at a 5 K·min^{-1} rate.

The last IL is the [C$_{12}$C$_1$im][PF$_6$] which was solid at room temperature, reaching liquid state, at 326 K (68 ºC). The same solid-solid transition observed previously in the other samples, appeared at 259 K (-14 ºC).
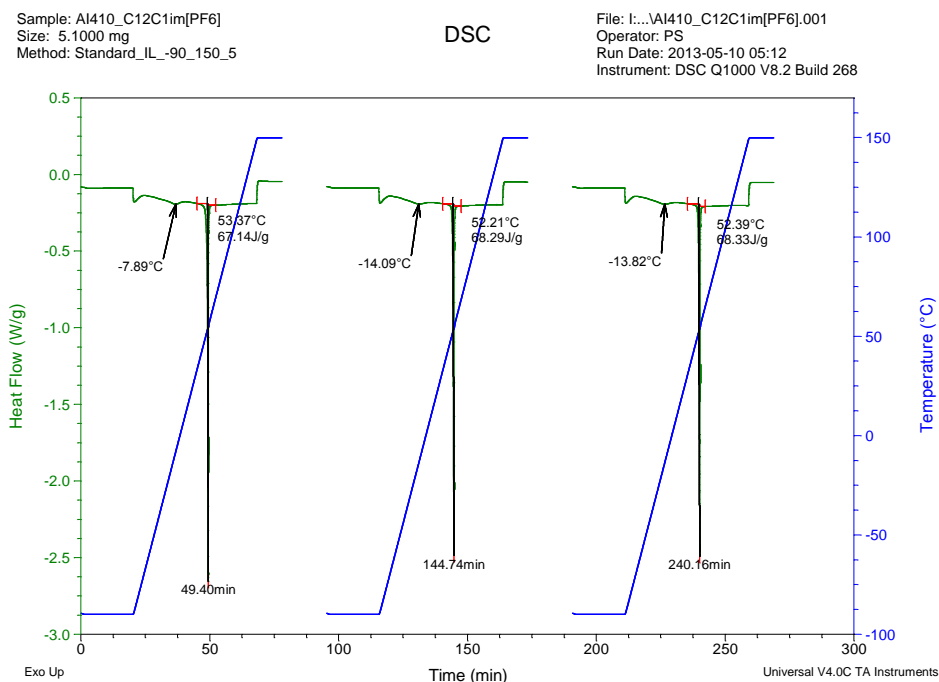
Figure 3.15 - Thermal analysis for [C$_{12}$C$_1$mim][PF$_6$] performed from 183 to 423 K, at a 5 K·min^{-1} rate.

3.1.3. Phase transitions summary

The phase transitions measured for 1-benzyl-3-methylimidazolium and alkylimidazolium series are presented in Table 3.1. The calculated T_g/T_m ratio is also presented, which is in reasonable agreement with eq. 1.8 and 1.9.

Table 3.1 - Phase transition temperatures: T_g, T_{s-s}, T_{cc} and T_m obtained using the TA Instruments Q1000 DSC.

Compound	T_g (K)	T_{s-s} (K)	T_{cc} (K)	T_m (K)	T_g/T_m
[Bnmim][BF$_4$]	235.3 ± 1.2	-	282.5 ± 0.1	336.5 ± 0.1	0.699
[Bnmim][PF$_6$]	244.8 ± 0.8	-	279.2 ± 0.2	399.7 ± 0.1	0.612
[Bnmim][C$_2$F$_4$HSO$_3$]	229.1 ± 0.5	-	260.1 ± 0.1	315.4 ± 0.1	0.726
[Bnmim][NTf$_2$]	216.7 ± 1.4	-	-	-	-
[C$_2$C$_1$im][PF$_6$]	-	232.3 ± 0.8	-	317.0 ± 0.7	-
[C$_3$C$_1$im][PF$_6$]	-	232.0 ± 0.2	-	311.8 ± 0.2	-
[C$_4$C$_1$im][PF$_6$]	196.0± 0.9	-	226.5[a]	285.3[a]	0.687
[C$_5$C$_1$im][PF$_6$]	199.2 ± 1.2	-	-	-	-
[C$_6$C$_1$im][PF$_6$]	201.7 ± 0.4	-	-	-	-
[C$_7$C$_1$im][PF$_6$]	203.5 ± 0.5	-	-	-	-
[C$_8$C$_1$im][PF$_6$]	203.5 ± 0.4	-	-	-	-
[C$_9$C$_1$im][PF$_6$]	205.9 ± 0.1	-	252.8 ± 0.5	293.0 ± 0.3	0.703
[C$_{10}$C$_1$im][PF$_6$]	208.2 ± 0.1	241.8 ± 0.8	238.8 ± 0.8	307.1 ± 0.1	0.678
[C$_{12}$C$_1$im][PF$_6$]	-	259.3 ± 0.1	-	326.5 ± 0.1	-

a
literature values obtained from Vilas *et al* [40]

The graphic representation of the phase transition temperatures against the number of carbons of the alkyl side chain of the 1-methyl-3-alkylimidazolium cation is presented in figure 3.16. From the analysis of figure 3.16, it can be observed that the melting, cold crystallization and solid-solid transition temperatures presents distinguished properties before and after the [C$_7$C$_1$im][PF$_6$]. The complex thermal behaviour observed in the [C$_7$C$_1$im][PF$_6$] indicates that the T$_{cc}$ and melting temperatures should be very near. That hypothesis is also supported by the observed trend depicted in figure 3.16. Due to their higher sphericity-like shape of the ionic pair, the ionic liquids with shorter alkyl side chains, C$_n$ (n = 2 and 3), have higher packing facility mechanism. That is in agreement with the observed thermal behaviour, where the crystallization occurs easily along the cooling step (no glass transition or crystallization on heating was observed) using the experimental procedure (thermal profile) adopted in this work. For intermediate region C$_n$ (n = 4, 5 and 6) with the increase of the alkyl chain size and consequently the steric hindrance of the ionic pair as well as, a significantly decrease of sphericity-like shape, the relative stability of the

crystalline phase decreases leading to a significant decrease on the melting temperature as observed in their thermal behaviour. After C_7, the alkyl chain organization lead to the formation of structured nonpolar domains and polar regions (in islands or channels format), leading to an increased stability of the crystalline phase and, as a consequence, an increase of the melting temperature along with the alkyl size increase, as obtained in the experimental results.

Experimental results recently reported by Vilas *et al* [40] for $[C_4C_1im][PF_6]$, were include in data presented in figure 3.16. In this work, several crystalline phases were found. The reported temperatures, enthalpies and melting temperatures refer to the crystalline phase less stable (at low temperatures), phenomenon that is usually found and obtained in the ILs. The considered crystalline phase becomes however the most stable at the melting temperature region [40].
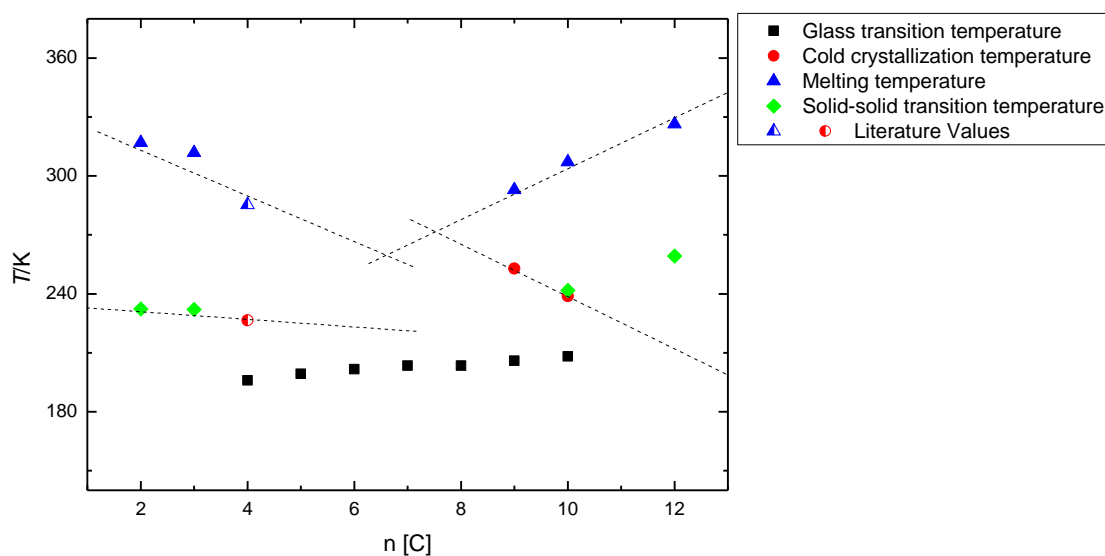
Figure 3.16 – Graphical representation of the T_g, $T_{s\text{-}s}$, T_{cc}, and T_m as a function of the number of carbons on the alkyl side chain of the $[C_nC_1im]^+$ cation.

3.1.4. Melting equilibria

In Table 3.2 is presented the results from phase transitions studies such as enthalpy (eq 3.1) and entropy (eq 3.2) of melting that can be computed through the experimental results of DSC.

$$\Delta H_{melting}(T_{melting}) = \frac{area_{melting} \cdot 10^{-3}}{n} \tag{3.1}$$

And from the enthalpies and temperature of melting, the entropies of melting could be derived.

$$\Delta S_{melting}(T_{melting}) = \frac{\Delta H_{melting}(T_{melting})}{T_{melting}(K)} \tag{3.2}$$

Table 3.2 – Melting temperature, entalpies and entropies of melting of the studied ILs.

IL	T_m (K)	ΔH_m (kJ·mol⁻¹)	ΔS_m (J·K⁻¹·mol⁻¹)
[Bnmim][BF$_4$]	336.5 ± 0.1	16.6 ± 0.6	49.4 ± 0.6
[Bnmim][PF$_6$]	399.7 ± 0.1	24.9 ± 1.3	62.2 ± 1.3
[Bnmim][C$_2$F$_4$HSO$_3$]	315.4 ± 0.1	23.6 ± 0.2	74.7 ± 0.3
[Bnmim][NTf$_2$]	-	-	-
[C$_2$C$_1$im][PF$_6$]	317.0 ± 0.7	15.3 ± 0.6	48.2 ± 0.9
[C$_3$C$_1$im][PF$_6$]	311.8 ± 0.2	15.7 ± 1.0	50.5 ± 1.0
[C$_4$C$_1$im][PF$_6$]¹	285.3[a]	13.1 ± 0.7[a]	45.9 ± 2.6[a]
[C$_5$C$_1$im][PF$_6$]	-	-	-
[C$_6$C$_1$im][PF$_6$]	-	-	-
[C$_7$C$_1$im][PF$_6$]	-	-	-
[C$_8$C$_1$im][PF$_6$]	-	-	-
[C$_9$C$_1$im][PF$_6$]	293.0 ± 0.3	17.0 ± 0.1	58.0 ± 0.3
[C$_{10}$C$_1$im][PF$_6$]	307.1 ± 0.1	19.3 ± 0.4	62.9 ± 0.4
[C$_{12}$C$_1$im][PF$_6$]	326.5 ± 0.1	26.5 ± 0.2	81.1 ± 0.3

a Values presented for this compound are obtained from literature [40]

Figure 3.17 and 3.18 presents the thermodynamic properties of melting against the number of carbons of the alkyl side chain of the cation for the 1-alkyl-3-methylimidazolium hexafluorophosphate ionic liquid series. The grey region represents the liquid ionic liquids for whose no melting was observed in the temperature range studied.
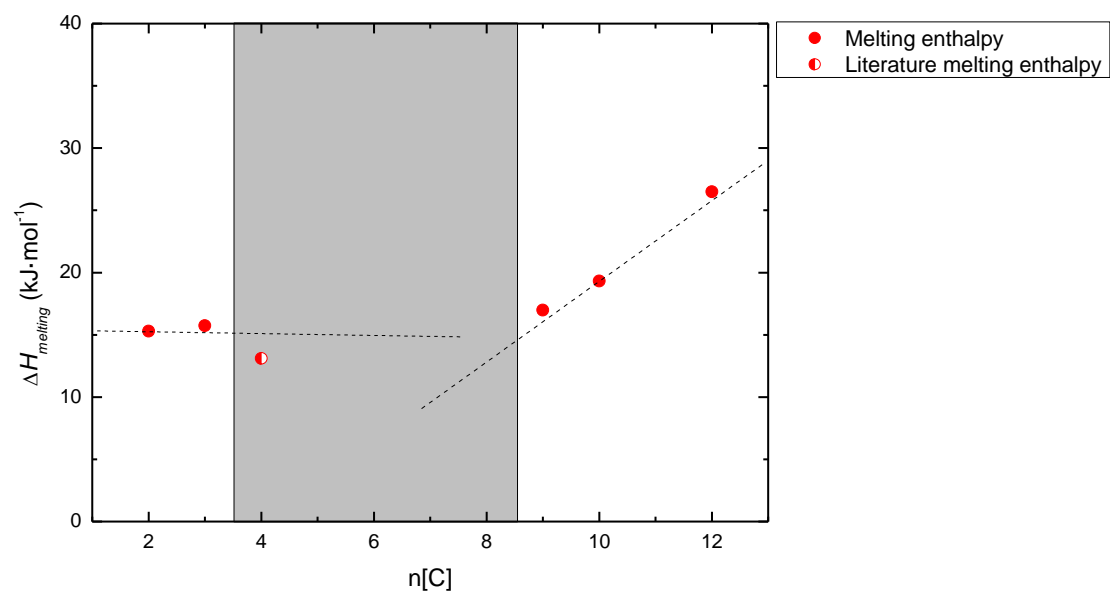
Figure 3.17 - Enthalpy dependence of the cation alkyl chain size, for melting.
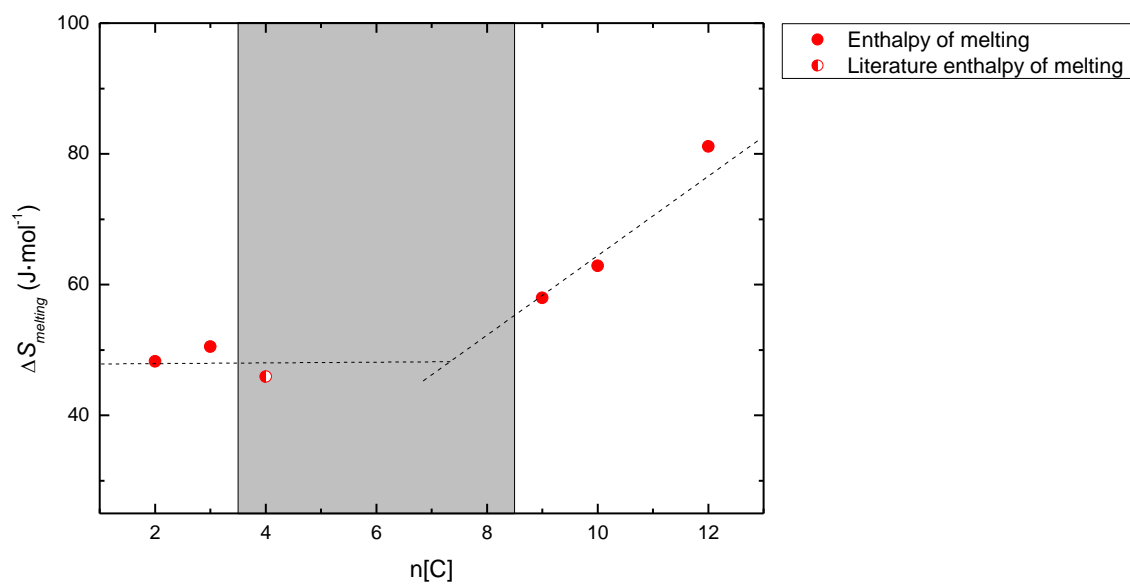
Figure 3.18 - Entropic dependence of the cation alkyl chain size, for melting.

3.2. Heat capacities

In this section is presented the heat capacity measurements performed in the μDSC IIIa. The scanning rate for step was 0.3 K·min^{-1} and 5 K·min^{-1} for continuous method, in the temperature range of 253 to 355 K. The heat capacities presented in the following tables are the average of the two independent measurements done for each method. The experimental data can be represented by a quadratic fit (eq.1.7):

$$C_{p,m}^{l}(T/K) = a + bT + cT^2 \qquad (3.3)$$

where a is in J·K^{-1}·mol^{-1}, b is in J·K^{-2}·mol^{-1} and c is in J·K^{-3}·mol^{-1}. The fit parameters (a, b, and c) were calculated from the step method. The standard deviation, σ, was calculated for the heat capacity obtained from the calculated parameters. [Bnmim][BF$_4$] (liquid phase) presented insufficient points for quadratic fit, being only computed the linear fit parameters.

Table 3.3 – Quadratic fit parameters for all the studied compounds, determined from step method measurements.

Compound	Phase	a (J·K^{-1}·mol^{-1})	b (J·K^{-2}·mol^{-1})	c(J·K^{-3}·mol^{-1})	σ^1
[Bnmim][BF$_4$]	Solid	545.4	-6.296	$1.217 \cdot 10^{-2}$	0.76
[Bnmim][BF$_4$]	Liquid	-	-	-	-
[Bnmim][PF$_6$]	Solid	153.7	0.882	$5.570 \cdot 10^{-5}$	0.43
[Bnmim][C$_2$F$_4$HSO$_3$]	Solid	1068.4	-5.319	$1.266 \cdot 10^{-2}$	0.94
[Bnmim][C$_2$F$_4$HSO$_3$]	Liquid	507.0	-0.470	$1.590 \cdot 10^{-3}$	0.45
[Bnmim][NTf$_2$]	Liquid	599.8	-0.148	$1.150 \cdot 10^{-3}$	0.62
[C$_2$C$_1$im][PF$_6$]	Solid	-51.0	-7.993	$1.658 \cdot 10^{-2}$	2.21
[C$_2$C$_1$im][PF$_6$]	Liquid	206.2	3.470	$-4.310 \cdot 10^{-3}$	5.58
[C$_3$C$_1$im][PF$_6$]	Solid	43.8	-2.529	$0.707 \cdot 10^{-2}$	1.43
[C$_3$C$_1$im][PF$_6$]	Liquid	526.9	-1.259	$2.590 \cdot 10^{-3}$	0.63
[C$_4$C$_1$im][PF$_6$]	Liquid	213.5	0.533	$6.156 \cdot 10^{-5}$	0.55
[C$_5$C$_1$im][PF$_6$]	Liquid	252.1	0.633	$-5.213 \cdot 10^{-5}$	0.46
[C$_6$C$_1$im][PF$_6$]	Liquid	285.7	0.601	$3.337 \cdot 10^{-5}$	0.57
[C$_7$C$_1$im][PF$_6$]	Liquid	354.3	0.330	$5.306 \cdot 10^{-4}$	0.90
[C$_8$C$_1$im][PF$_6$]	Liquid	346.0	0.595	$1.339 \cdot 10^{-4}$	0.66
[C$_9$C$_1$im][PF$_6$]	Liquid	356.1	0.817	$-1.918 \cdot 10^{-4}$	0.86
[C$_{10}$C$_1$im][PF$_6$]	Solid	1642.5	-5.246	$1.176 \cdot 10^{-2}$	0.46
[C$_{10}$C$_1$im][PF$_6$]	Liquid	604.4	-0.591	$1.960 \cdot 10^{-3}$	0.71
[C$_{12}$C$_1$im][PF$_6$]	Solid	5485.2	-36.56	$0.659 \cdot 10^{-1}$	1.49
[C$_{12}$C$_1$im][PF$_6$]	Liquid	909.2	-2.091	$4.320 \cdot 10^{-3}$	0.05

$$^1\sigma = \left[\sum_{i=1}^{n} \left(C_{p,m}^{exp} - C_{p,m}^{lf} \right)_i^2 \Big/ (n-m) \right]^{1/2}$$, where n is the number of fitted data points and m is the number of

adjustable parameters.

However, for the ionic liquids measured, the studied temperature range is short and only a linear fit was considered:

$$C_{p,m}^{l}(T/K) = a + bT \tag{3.4}$$

where a is in $J \cdot K^{-1} \cdot mol^{-1}$ and b is in $J \cdot K^{-2} \cdot mol^{-1}$. The fit parameters ($a$ and b) were calculated from the step method. The mean deviation, σ, was calculated for the heat capacity results obtained from the step method.

Table 3.4 - Linear fit parameters for all the studied compounds, determined from step method values.

Compound	Phase	a ($J \cdot K^{-1} \cdot mol^{-1}$)	b ($J \cdot K^{-2} \cdot mol^{-1}$)	σ^1
[Bnmim][BF$_4$]	Solid	6.2	0.9665	1.01
[Bnmim][BF$_4$]	Liquid	230.5	0.5436	0.05
[Bnmim][PF$_6$]	Solid	87.1	0.9058	0.76
[Bnmim][C$_2$F$_4$HSO$_3$]	Solid	-204.2	1.7502	1.69
[Bnmim][C$_2$F$_4$HSO$_3$]	Liquid	322.8	0.6317	0.20
[Bnmim][NTf$_2$]	Liquid	448.5	0.5402	1.35
[C$_2$C$_1$im][PF$_6$]	Solid	-47.3	1.2683	1.04
[C$_2$C$_1$im][PF$_6$]	Liquid	199.7	0.4759	0.05
[C$_3$C$_1$im][PF$_6$]	Solid	-25.3	1.3331	0.17
[C$_3$C$_1$im][PF$_6$]	Liquid	230.2	0.4883	0.26
[C$_4$C$_1$im][PF$_6$]	Liquid	260.5	0.5070	0.64
[C$_5$C$_1$im][PF$_6$]	Liquid	257.4	0.6008	0.46
[C$_6$C$_1$im][PF$_6$]	Liquid	283.2	0.6217	0.57
[C$_7$C$_1$im][PF$_6$]	Liquid	305.6	0.6549	1.00
[C$_8$C$_1$im][PF$_6$]	Liquid	334.2	0.6773	0.67
[C$_9$C$_1$im][PF$_6$]	Liquid	358.6	0.7052	0.93
[C$_{10}$C$_1$im][PF$_6$]	Solid	216.8	0.8483	2.99
[C$_{10}$C$_1$im][PF$_6$]	Liquid	385.9	0.7308	0.49
[C$_{12}$C$_1$im][PF$_6$]	Solid	180.2	0.9606	1.10
[C$_{12}$C$_1$im][PF$_6$]	Liquid	392.9	0.8587	0.27

$^1 \sigma = \left[\sum_{i=1}^{n} \left(C_{p,m}^{exp} - C_{p,m}^{lf} \right)_{i}^{2} \Big/ (n-m) \right]^{1/2}$, where n is the number of fitted data points and m is the number of

adjustable parameters.

3.2.1. Heat capacity of 1-benzyl-3-methylimidazolium hexafluorophosphate

Figure 3.19 presents the deviations from the fitting data obtained, step measurements and continuous measurements for [Bnmim][PF$_6$]. The measurements were performed from 253 to 355 K at 0.3 K·min^{-1}. The results presented are the average from the measurements performed. "0 line" stands for the values obtained by quadratic fit (parameters are presented in table 3.3 and 3.4). The fitting parameters were determined from step method measurements.

Figure 3.19 - Relative deviation of the experimental heat capacities C_p^{exp} for [Bnmim][PF$_6$] from the smoothed values C_p^{lf}. The black line represents the continuous method values and the squares are step method results. "0 line" stands for the values obtained by quadratic fit (parameters are presented in table 3.3).

The experimental values of the molar heat capacity for [Bnmim][PF$_6$] in the range 278 to 355 K and deviations are given in Table 3.5. Each value corresponds to the average of two independent measurements, using step and continuous methods. The deviation from the quadratic fit is presented for both methods. The parameters a, b and c were obtained from the fitting of the step method values ($C_{p,m}^{s}(T) = 153.7 - 0.882 \cdot T + 5.570 \cdot 10^{-5} \cdot T^2$ from quadratic fit *and $C_{p,m}^{s}(T) = 87.1 + 0.9058 \cdot T$* for linear fit).

Additionally, the effect of water on the heat capacities measurements was evaluated for the studied ionic liquid. Table 3.5 lists the molar heat capacities for dried and the same sample before drying.

Table 3.5 - Experimental molar heat capacities ($J \cdot K^{-1} \cdot mol^{-1}$) for solid [Bnmim][PF$_6$] (dried and not dried sample) and the data derived from quadratic fitting for both step and continuous method.

| | Dried Sample | | | | | Not dried sample | | | |
| | Step method | | | Continuous method | | Step method | | Continuous method | |
T/K	$C_{p,m}$	Quadratic fit	% dev.	$C_{p,m}$	% dev.	$C_{p,m}$	% dev.	$C_{p,m}$	% dev.
258.09	321.08	320.75	0.10	321.68	0.21	317.55	-1.06	318.51	-0.76
263.20	324.93	325.42	-0.15	326.45	0.27	321.69	-1.19	323.60	-0.59
268.30	329.76	330.10	-0.10	331.03	0.27	326.46	-1.19	328.37	-0.60
273.41	335.03	334.77	0.08	336.25	0.46	331.55	-0.92	334.42	-0.11
278.51	339.71	339.45	0.08	339.94	0.20	336.33	-0.88	338.55	-0.23
283.62	344.65	344.13	0.15	344.18	0.10	341.10	-0.83	343.33	-0.16
288.72	348.73	348.81	-0.02	348.21	-0.06	345.69	-0.88	348.42	-0.04
293.83	353.16	353.49	-0.09	352.52	-0.12	349.69	-0.94	353.51	0.14
298.93	358.03	358.16	-0.04	356.30	-0.35	354.15	-0.94	357.33	-0.10
304.04	362.79	362.84	-0.02	360.70	-0.39	358.92	-0.90	360.83	-0.35
309.14	367.39	367.52	-0.04	364.92	-0.48	363.37	-0.86	363.37	-0.87
314.25	372.53	372.20	0.09	369.82	-0.38	368.46	-0.78	367.19	-1.10
319.35	377.53	376.87	0.17	374.87	-0.24	373.56	-0.59	371.65	-1.07
324.46	381.58	381.55	0.01	379.03	-0.35	377.37	-0.76	375.78	-1.15
329.56	385.86	386.23	-0.10	383.75	-0.30	381.51	-0.94	379.92	-1.33
334.67	390.32	390.90	-0.15	389.15	-0.09	385.65	-0.97	385.01	-1.12
339.77	395.05	395.58	-0.14	394.23	0.05	390.10	-0.96	389.78	-1.07
344.88	399.94	400.26	-0.08	399.77	0.29	394.56	-1.07	394.24	-1.12
349.98	405.06	404.94	0.03	404.77	0.40	399.01	-0.99	398.69	-1.12
355.09	410.45	409.61	0.20	410.81	0.76	403.46	-1.03	403.78	-0.90

Figure 3.20 depicts the relative deviation of the experimental heat capacities and the values obtained from the fitting, for a sample not dried.
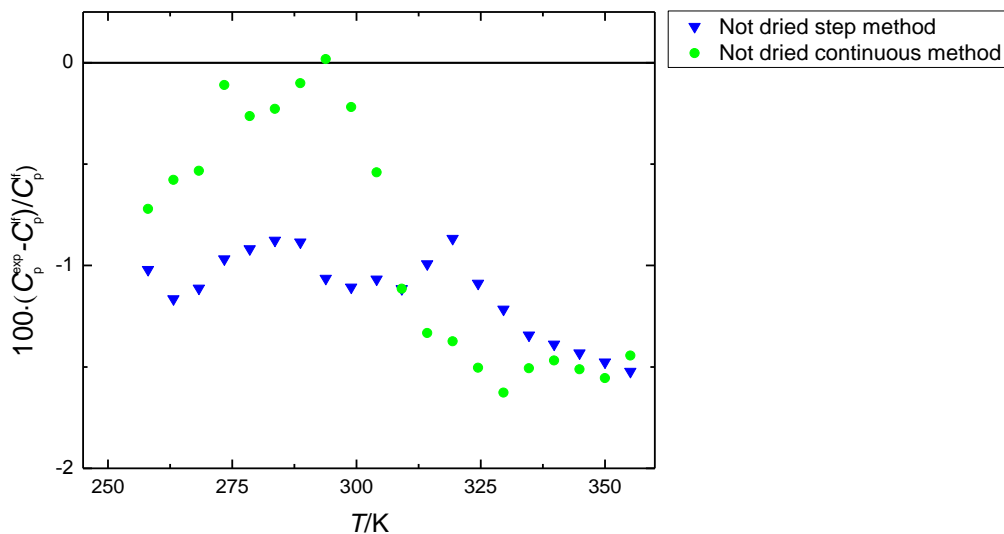
Figure 3.20 - Relative deviation of the experimental heat capacities C_p^{exp} for [Bnmim][PF$_6$] not dried, from the smoothed values C_p^{lf}. "0 line" stands for the values obtained by quadratic fit (parameters are presented in table 3.3).

When compared with the dried sample values, it was found that the heat capacity values are lower in the presence of water, as shown in Figure 3.21 (the water content was lower than 1% before drying). In blue and in green are represented the values for the same sample but not dried (in blue the continuous method and in green the step method). "0 line" stands for the values obtained by quadratic fitting.
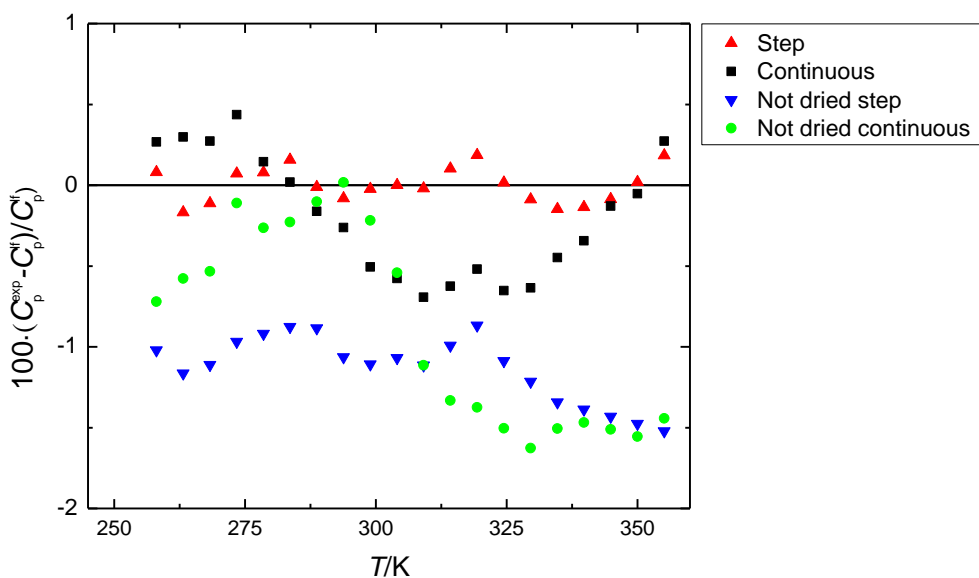
Figure 3.21 - Relative deviation of the experimental heat capacities, C_p^{exp}, for [Bnmim][PF$_6$] from the fit values, C_p^{lf}, for both dried and not dried samples. "0 line" stands for the values obtained by quadratic fit (parameters are presented in table 3.3).

3.2.2. Heat capacity of 1-benzyl-3-methylimidazolium tetrafluoroborate

Figure 3.22 presents the fitting data obtained from step and continuous measurements for [Bnmim][BF$_4$]. The measurements were performed from 253 to 355 K at 0.3 K·min^{-1}. The results presented are the average from the measurements performed. A phase transition was detected at 336 K represented by the dashed vertical line. "0" stands for the values obtained by quadratic fit (parameters are presented in table 3.3 and 3.4). The fitting parameters were determined from step method measurements.
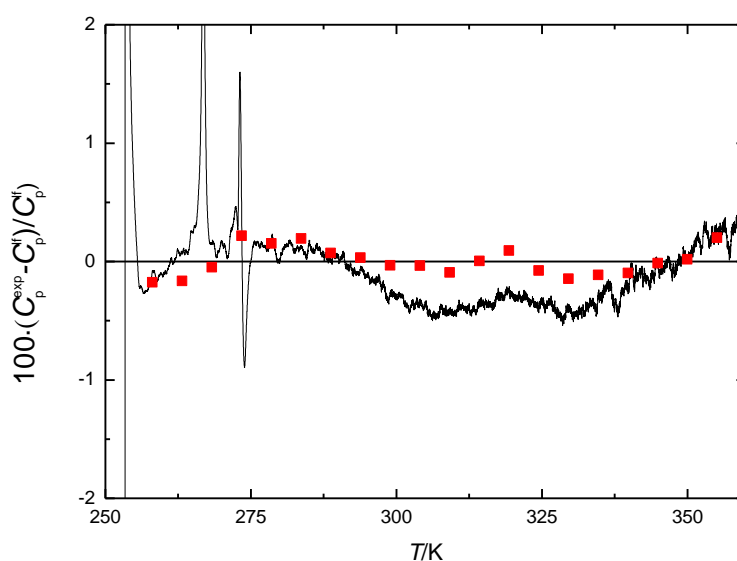

Figure 3.22 - Relative deviation of the experimental heat capacities C_p^{exp} for [Bnmim][BF$_4$] from the smoothed values C_p^{lf}. The black line represents the continuous method values and the squares are step method results. "0 line" stands for the values obtained by quadratic fit (parameters are presented in table 3.3).

The experimental values of the molar heat capacity for [Bnmim][BF$_4$] in the range 278 to 355 K and deviations are given in Table 3.6. Each value corresponds to the average of two independent measurements, using step and continuous methods. The deviation from the quadratic fit is presented for both methods. The parameters *a*, *b* and *c* were obtained from the fitting of the step method values ($C_{p,m}^s(T)$ = 545.4-6.296·T+1.217·10^{-2}·T^2 from quadratic fit *and* $C_{p,m}^l(T)$= 230.5+0.5436·T and $C_{p,m}^s(T)$= 6.2+0.9665·T for linear fit). The heat capacity values measured in the temperature range of 258 to 278 K and 334 to 339 K are not presented due to phase transitions occurring in those temperature ranges.

Table 3.6 - Experimental molar heat capacities ($J \cdot K^{-1} \cdot mol^{-1}$) for solid and liquid phases of [Bnmim][BF$_4$] and results derived from fitted equation for both step and continuous method.

T/K	Step method			Continuous method	
	$C_{p,m}$	Quadratic fit	% dev.	$C_{p,m}$	% dev.
258.09	-	-	-	-	-
263.20	-	-	-	-	-
268.30	-	-	-	-	-
273.41	-	-	-	-	-
278.51	288.03	287.24	0.28	295.05	1.96
283.62	292.27	291.69	0.20	298.34	2.18
288.72	296.71	296.32	0.13	301.33	1.99
293.83	301.12	301.11	0.00	302.58	1.17
298.93	305.96	306.08	-0.04	303.72	0.06
304.04	310.73	311.21	-0.15	307.82	-0.56
309.14	316.25	316.53	-0.09	315.20	-0.15
314.25	322.04	322.01	0.01	323.99	0.58
319.35	327.54	329.66	-0.64	331.66	-0.76
324.46	334.79	333.49	0.39	337.09	0.08
329.56	-	-	-	-	-
334.67	-	-	-	-	-
339.77	-	-	-	-	-
344.88	417.85	417.93	-0.02	417.44	-0.12
349.98	420.89	420.71	0.04	419.96	-0.22
355.09	423.40	423.48	-0.02	423.30	-0.04

3.2.3. Heat capacity of 1-benzyl-3-methylimidazolium 1,1,2,2-tetrafluoroethanesulfonate

Figure 3.23 presents the fitting data obtained from step and continuous measurements for [Bnmim][$C_2F_4HSO_3$]. The measurements were performed from 253 to 355 K at 0.3 K·min^{-1}. The results presented are the average from the measurements performed. A phase transition was detected at 314 K represented by the dashed vertical line. "0 line" stands for the values obtained by quadratic fit (parameters are presented in table 3.3 and 3.4). The fitting parameters were determined from step method measurements. Continuous method data was removed due to an error occurring along the measurements.

Figure 3.23 - Relative deviation of the experimental molar heat capacities C_p^{exp} for [Bnmim][$C_2F_4HSO_3$] for step method. The squares are step method results. "0 line" stands for the values obtained by quadratic fit (parameters are presented in table 3.3).

The experimental values of the molar heat capacity for [Bnmim] [$C_2F_4HSO_3$] in the range 278 to 355 K and deviations are given in Table 3.7. Each value corresponds to the average of two independent measurements, using step and continuous methods. The deviation from the quadratic fit is presented for both methods. The parameters *a*, *b* and *c* were obtained from the fitting of the step method values ($C^s_{p,m}(T) = 1068.4 - 5.319 \cdot T + 1.266 \cdot 10^{-2} \cdot T^2$ and $C^l_{p,m}(T) = 507.0 - 0.470 \cdot T + 1.590 \cdot 10^{-3} \cdot T^2$ for quadratic fit *and $C^s_{p,m}(T) = -204.2 + 1.7502 \cdot T$ and $C^l_{p,m}(T) = 322.8 + 0.6317 \cdot T$* for linear fit). The heat capacity values measured in the temperature range of 258 to 268 K and 314 to 319 K are not presented due to phase transitions occurring in those temperature ranges.

Table 3.7 - Experimental molar heat capacities ($J \cdot K^{-1} \cdot mol^{-1}$) for solid and liquid phases of [Bnmim][$C_2F_4HSO_3$] and results derived from fitted equation for both step and continuous method.

| T/K | Step method | | | Continuous method | |
	$C_{p,m}$	Quadratic fit	% dev.	$C_{p,m}$	% dev.
258.09	-	-	-	-	-
263.20	-	-	-	-	-
268.30	-	-	-	-	-
273.41	380.59	379.77	0.22	392.30	3.30
278.51	388.59	389.46	-0.22	398.39	2.29
283.62	398.36	399.62	-0.32	405.78	1.54
288.72	407.11	410.22	-0.76	415.37	1.26
293.83	422.95	421.30	0.39	423.94	0.63
298.93	436.35	432.81	0.82	434.12	0.30
304.04	441.43	444.80	-0.76	447.89	0.70
309.14	456.94	457.22	-0.06	-	-
314.25	-	-	-	-	-
319.35	-	-	-	-	-
324.46	521.83	521.50	0.06	526.72	1.00
329.56	524.50	524.62	-0.02	529.72	0.97
334.67	527.44	527.75	-0.06	526.72	-0.20
339.77	530.80	530.87	-0.01	529.72	-0.21
344.88	533.96	534.00	-0.01	532.99	-0.19
349.98	537.23	537.12	0.02	537.01	-0.02
355.09	540.35	540.26	0.02	540.70	0.08

3.2.4. Heat capacity of 1-benzyl-3-methylimidazolium bis(trifluoromethylsulfonyl)imide.

In Figure 3.24 is presented the fitting data obtained from step and continuous measurements for [Bnmim][NTf$_2$]. The measurements were performed from 253 to 355 K at 0.3 K·min^{-1}. The results presented are the average from the measurements performed. "0" stands for the values obtained by quadratic fit (parameters are presented in table 3.3 and 3.4). The fitting parameters were determined from step method measurements.
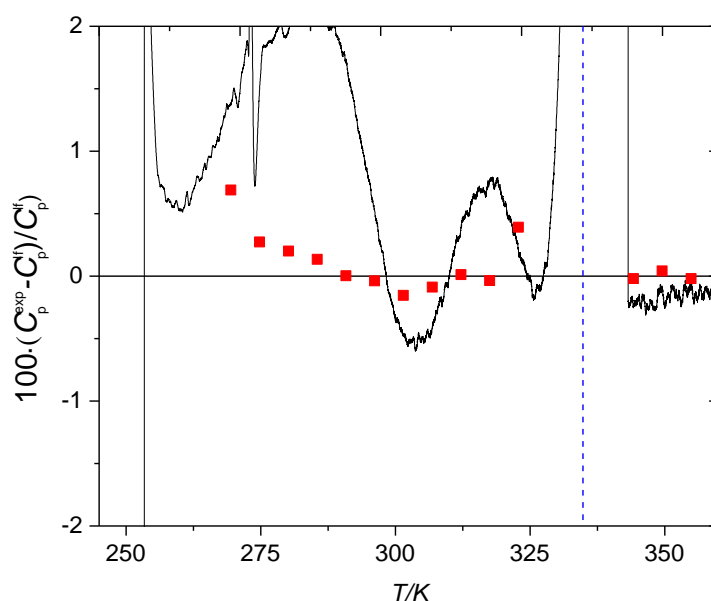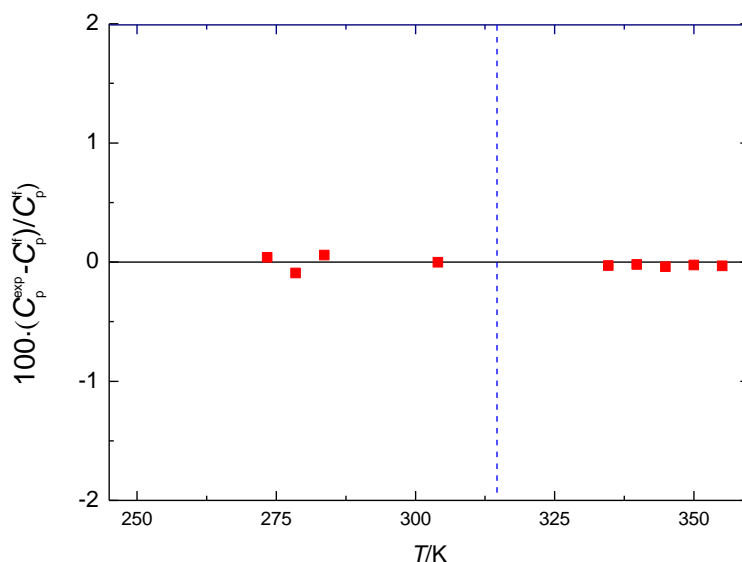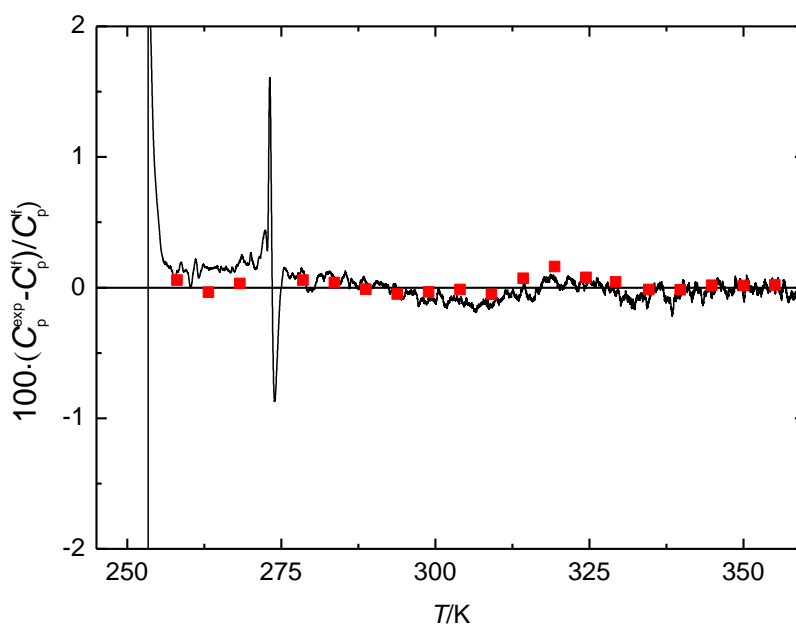

Figure 3.24 - Relative deviation of the experimental molar heat capacities C_p^{exp} for [Bnmim][NTf$_2$] for step method. The squares are step method results. "0 line" stands for the values obtained by quadratic fit (parameters are presented in table 3.3).

The experimental values of the molar heat capacity for [Bnmim][NTf$_2$] in the range 278 to 355 K and deviations are given in Table 3.8. Each value corresponds to the average of two independent measurements, using step and continuous methods. The deviation from the quadratic fit is presented for both methods. The parameters *a*, *b* and *c* were obtained from the fitting of the step method values ($C^l_{p,m}(T)$ = 599.8 -0.148·T+1.150·10^{-3}·T^2 from quadratic fit *and $C^l_{p,m}(T)$= 448.5 +0.5402·T* for linear fit).

Table 3.8 - Experimental molar heat capacities (J·K^{-1}·mol^{-1}) for liquid [Bnmim][NTf$_2$] and results derived from fitted equation for both step and continuous method.

T/K	$C_{p,m}$	Step method Quadratic fit	% dev.	Continuous method $C_{p,m}$	% dev.
258.09	587.80	585.33	0.42	588.65	0.19
263.20	588.75	588.16	0.10	590.85	-0.13
268.30	591.75	590.99	0.13	593.41	-0.17
273.41	594.37	593.82	0.09	599.39	-0.15
278.51	596.27	596.65	-0.06	597.51	-0.21
283.62	599.16	599.49	-0.06	599.69	-0.28
288.72	601.32	602.32	-0.17	601.86	-0.38
293.83	603.68	605.15	-0.24	604.13	-0.46
298.93	606.86	607.98	-0.18	606.39	-0.40
304.04	609.81	610.81	-0.16	609.02	-0.38
309.14	612.46	613.64	-0.19	611.43	-0.40
314.25	615.97	616.47	-0.08	615.08	-0.29
319.35	619.54	619.30	0.04	618.40	-0.17
324.46	621.92	622.13	-0.03	620.92	-0.24
329.56	624.68	624.97	-0.05	623.45	-0.25
334.67	627.43	627.80	-0.06	626.55	-0.26
339.77	630.49	630.63	-0.02	629.83	-0.22
344.88	634.11	63346	0.10	633.12	-0.09
349.98	637.55	636.29	0.20	636.32	0.00
355.09	640.60	639.12	0.23	640.07	0.04

3.2.5. 1- benzyl-3-methylimidazolium heat capacities general trends

The solid and liquid molar heat capacities at 298.15 K for the [Bnmim] series are summarized in Table 3.9.

Table 3.9 – Solid and liquid molar heat capacities of the [Bnmim] series at 298.15 K and respective molar weight.

Compound	M (g·mol^{-1})	$C^s_{p,m}$ (J·K^{-1}·mol^{-1})	$C^l_{p,m}$ (J·K^{-1}·mol^{-1})
[Bnmim][BF$_4$]	260.04	305.96 ± 0.22	393.0 ± 0.70
[Bnmim][PF$_6$]	318.20	357.17 ± 0.86	-
[Bnmim][C$_2$F$_4$HSO$_3$]	354.32	435.23 ± 1.11	503.31 ± 1.61
[Bnmim][NTf$_2$]	453.38	-	606.63 ± 0.24

Figure 3.25 depicts the apparent heat capacity for [Bnmim][BF$_4$], [Bnmim][PF$_6$], [Bnmim][C$_2$F$_4$HSO$_3$], and [Bnmim][NTf$_2$] and Figure 3.26 presents the correlated heat capacity. In the grey zones, can be seen that the ΔC_p is about 60 J·K^{-1}·mol^{-1}, a common value for molecular solids.
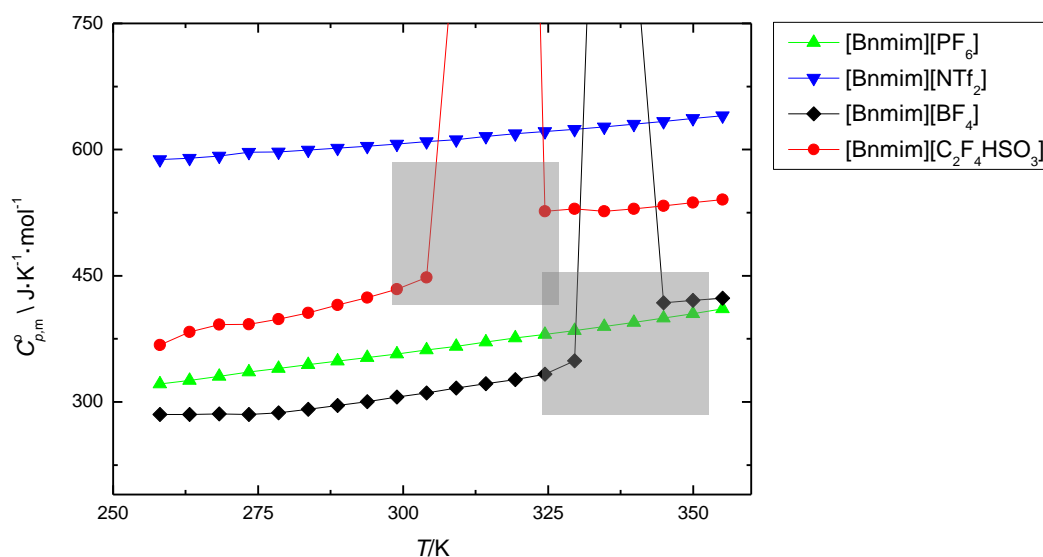
Figure 3.25 – Molar heat capacity dependence with the temperature, for [Bnmim][PF$_6$], [Bnmim][NTf$_2$], [Bnmim][BF$_4$], and [Bnmim][C$_2$F$_4$HSO$_3$]. All compounds were studied under the same experimental conditions.

In Figure 3.26 can be observer that solid heat capacities present a similar tendency, different from the tendency presented by the liquid phase heat capacities from the same ILs.
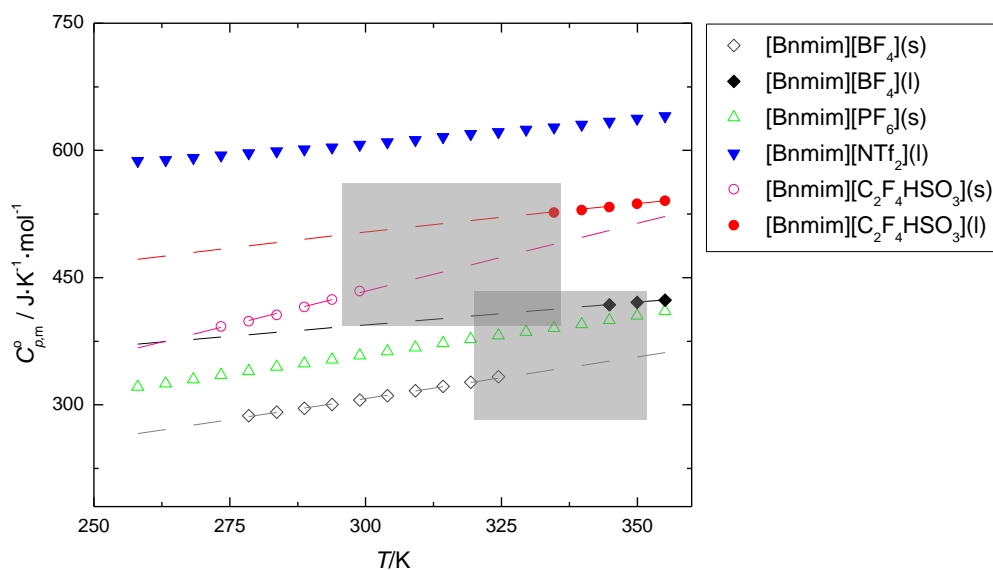
Figure 3.26 - Heat capacity dependence with temperature of [Bnmim][PF$_6$], [Bnmim][NTf$_2$], [Bnmim][BF$_4$], and [Bnmim][C$_2$F$_4$HSO$_3$]. The dashed lines are extrapolations made for each physical state (solid and liquid).

3.2.6. Heat capacities of the 1-alkyl-3-methylimidazolium series

Table 3.10 presents the heat capacities at 298 K measured in Setaram μDSC IIIa (step mode, for the range 253 – 355 K at 0.3 K·min^{-1}) are summarized. For the compounds exhibiting phase transitions at 298 K, their heat capacity was extrapolated from liquid phase to 298 K. The extrapolated data was calculated considering the parameters presented in Table 3.3 and Table 3.4. All the measurements were performed under the same experimental conditions.

Table 3.10 – Molar heat capacities for the 1-alkyl-3-methylimidazolium serie at 298.15 K and respective molar weight.

Compound	M (g mol^{-1})	$C^s_{p,m}$ (J·K^{-1}·mol^{-1})	$C^l_{p,m}$ (J·K^{-1}·mol^{-1})
[C$_2$C$_1$im][PF$_6$]	256.06	330.87 ± 0.23	346.63 ± 0.29
[C$_3$C$_1$im][PF$_6$]	270.07	378.54 ± 0.40	371.37 ± 5.79
[C$_4$C$_1$im][PF$_6$]	284.09	-	411.64 ± 0.97
[C$_5$C$_1$im][PF$_6$]	298.09	-	436.82 ± 0.06
[C$_6$C$_1$im][PF$_6$]	312.10	-	468.62 ± 0.13
[C$_7$C$_1$im][PF$_6$]	326.11	-	500.02 ± 0.13
[C$_8$C$_1$im][PF$_6$]	340.12	-	536.19 ± 0.04
[C$_9$C$_1$im][PF$_6$]	354.13	-	569.15 ± 0.10
[C$_{10}$C$_1$im][PF$_6$]	368.14	651.87 ± 12.84	600.36 ± 0.01
[C$_{12}$C$_1$im][PF$_6$]	394.16	630.01 ± 0.08	660.01 ± 0.47

The experimental data is compiled, compared and presented in Figure 3.27 (for apparent heat capacity) and in Figure 3.28 (correlated data).
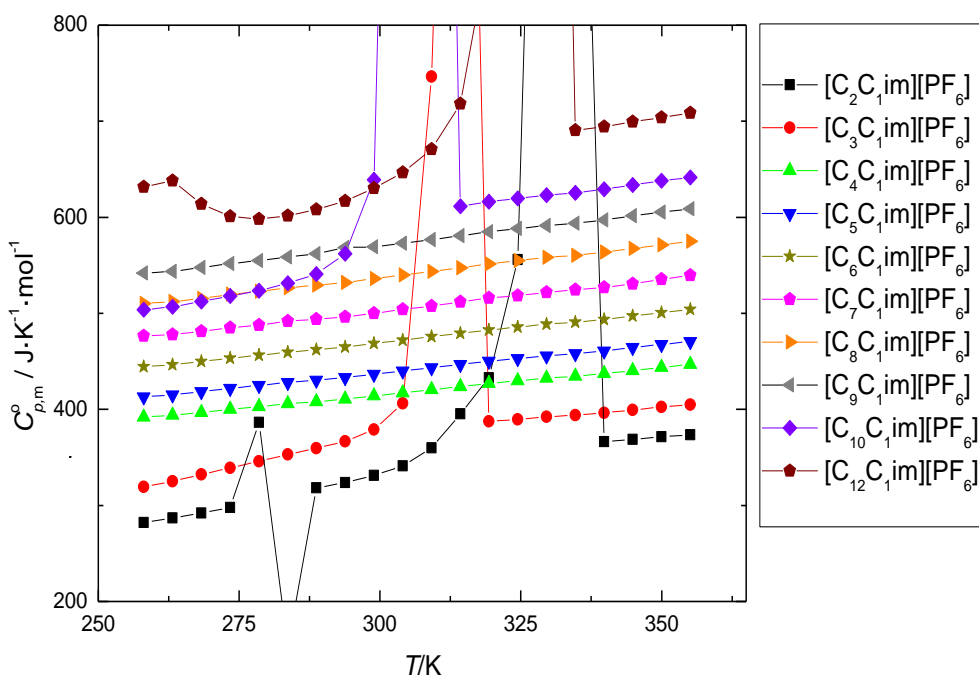
Figure 3.27 - Apparent molar heat capacities, at 298 K, as temperature function for the [C$_n$C$_1$im] studied, where n = 2 - 10 and 12.

In Figure 3.28 can be observed that the liquid phase heat capacities are equally separated from each other (values for C$_4$ are too high, and in error therefore), presenting similar slopes for their values.
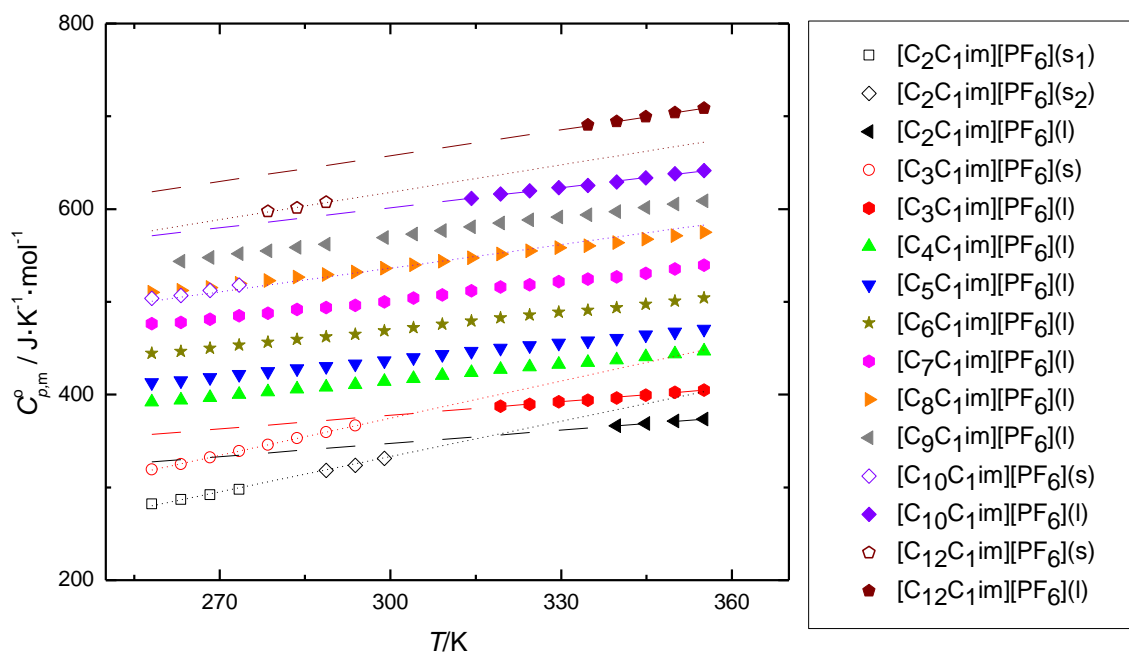
Figure 3.28 – Molar heat capacities as temperature function, at 298.15 K, for the [C$_n$C$_1$im][PF$_6$] studied, where n = 2 - 10 and 12 (empty symbols are for solid phase and full symbols are for liquid phase).

3.2.7. Temperature dependence on heat capacities

In Figure 3.29 is represented the temperature dependence on heat capacities for their liquid phase, at 355 K. It can be seen that the heat capacity increases with the increasing of alkyl side chain length.
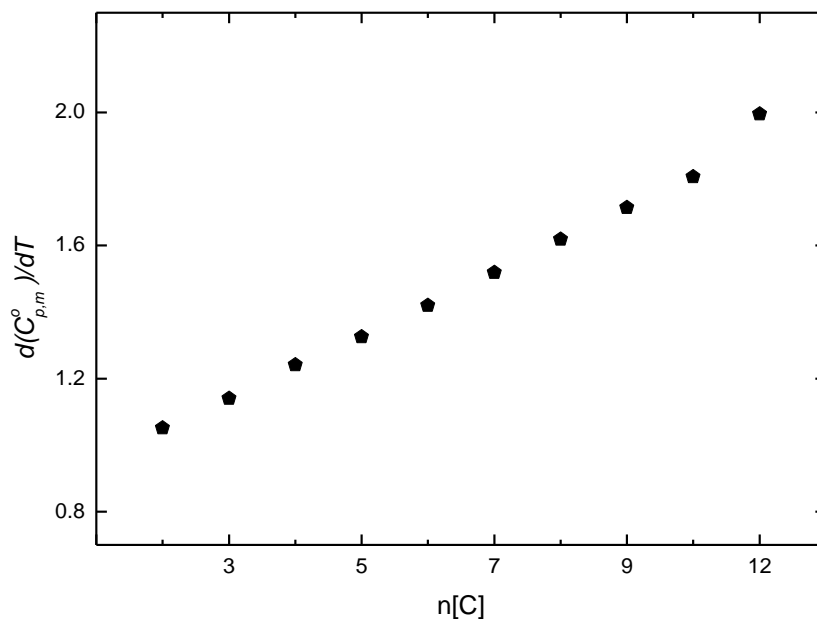
Figure 3.29 - Temperature dependence on $[C_nC_1im][PF_6]$ (where n = 2-10 and 12) the molar heat capacities, at 355 K, in the liquid phase as function of the side alkyl chain.

3.2.8. Anion effect on heat capacities

To better demonstrate the anion effect, a comparison was made with the literature data by Rocha *et al* [41], where the heat capacities for the $[C_nC_1im][NTf_2]$ is reported (Figure 3.30 and Figure 3.31). It is obvious that the molar weight play an important role in heat capacity, since NTf_2 $[C^{\circ}_{p,m}$ (T/K) = 439.9(±1.2)+31.50(±0.17)$T]$ is a higher due to the large number of atoms in the anion than PF_6 $[C^{\circ}_{p,m}$ (T/K) = 282.2(±2.5)+31.46(±0.35)$T]$, resulting in higher heat capacity values. Taking into account that C_2, C_4, C_{10} and C_{12} ionic liquids are solid at 298.15 K, an extrapolation was made for liquid heat capacities comparison.
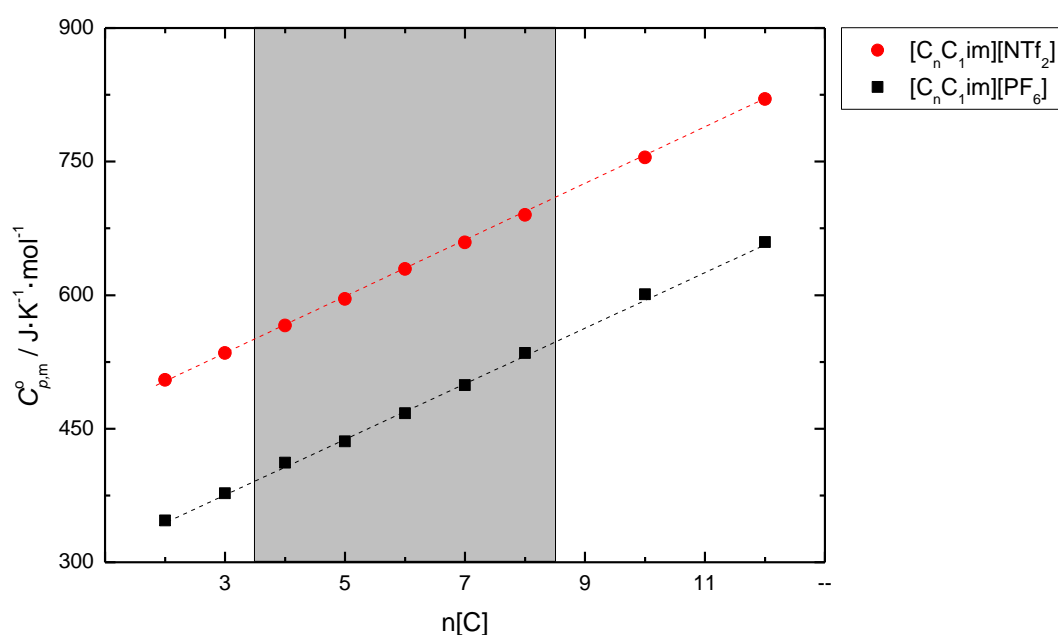
Figure 3.30 - Molar heat capacities, at T = 298.15 K, as function of the number of carbon atoms in the alkyl side chain of the cation, n(C), for $[C_nC_1im][PF_6]$ (with n = 2 – 8, 10, 12) and $[C_nC_1im][NTf_2]$ (with n = 2 – 8, 10, 12).

The heat capacity increment of the methylene group, $-CH_2-$, is identical in both ILs series, 32.4 ± 2.5 $J \cdot K^{-1} \cdot mol^{-1}$ for the $[C_nC_1im][PF_6]$ and 30.6 ± 1.3 $J \cdot K^{-1} \cdot mol^{-1}$ for $[C_nC_1im][NTf_2]$ series.

Figure 3.31, presents a comparison between specific heat capacities of the [$C_nC_1$im][NTf$_2$] series reported by Rocha *et al* [41], and the results obtained in this work for the [$C_nC_1$im][PF$_6$] series. The PF$_6$ series presents higher specific heat capacity than the NTf$_2$ Series.

Figure 3.31 - Specific heat capacities, at T = 298.15 K, as function of the number of carbon atoms in the alkyl side chain of the cation, n(C), for [$C_nC_1$im][PF$_6$] (with n = 2 – 8, 10, 12) and [$C_nC_1$im][NTf$_2$] (with n = 2 – 8, 10, 12).

In Figure 3.32, the volumic heat capacity dependence on the number of carbons of the alkyl side chain of the cation for the [$C_nC_1$im][PF$_6$] and [$C_nC_1$im][NTf$_2$] ionic liquid series is represented. The volumic heat capacities, C_p/V, for the [$C_nC_1$im][PF$_6$] were calculated taking into account the specific heat capacities and the density data available in the literature. [40] C_p/V data for the [$C_nC_1$im][NTf$_2$] ionic liquid series was recently reported in the literature by Rocha *et al* [39, 42]. The results will be evaluated based on a comparative analysis with the [$C_nC_1$im][NTf$_2$] in order to explore the effect of the anion on the heat capacity data.

A trend shift around C_6 and C_7 was found along the volumic heat capacity with the alkyl side chain length for PF_6. For shorter alkyl chain length size, the volumic heat capacity decreases with the increase of the alkyl chain size. After C_7, the volumic heat capacities reaches a stationary value of 1.94 $J \cdot K^{-1} \cdot cm^{-3}$, slightly higher than the identical behaviour observed in the $[C_nC_1im][NTf_2]$ IL series (1.92 $J \cdot K^{-1} \cdot cm^{-3}$)[42].

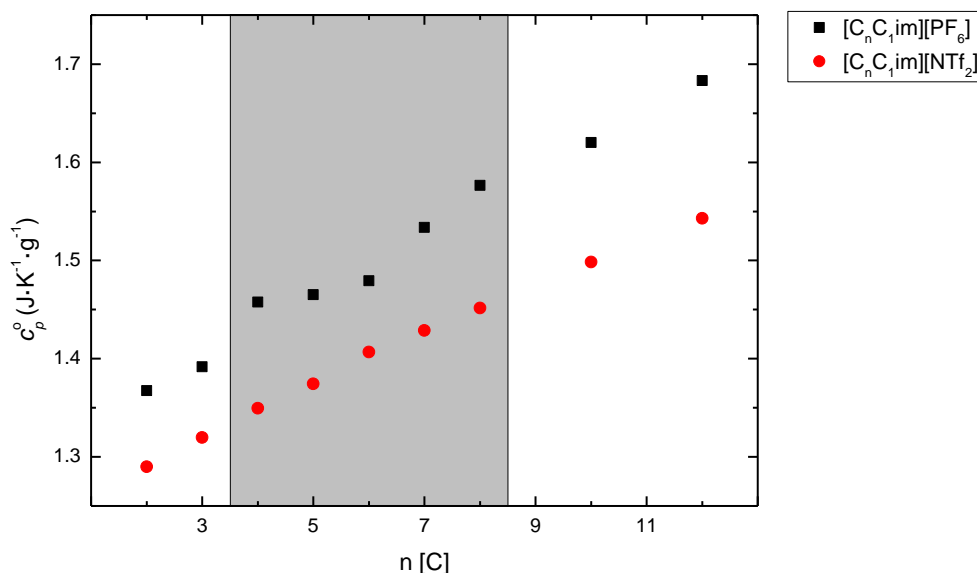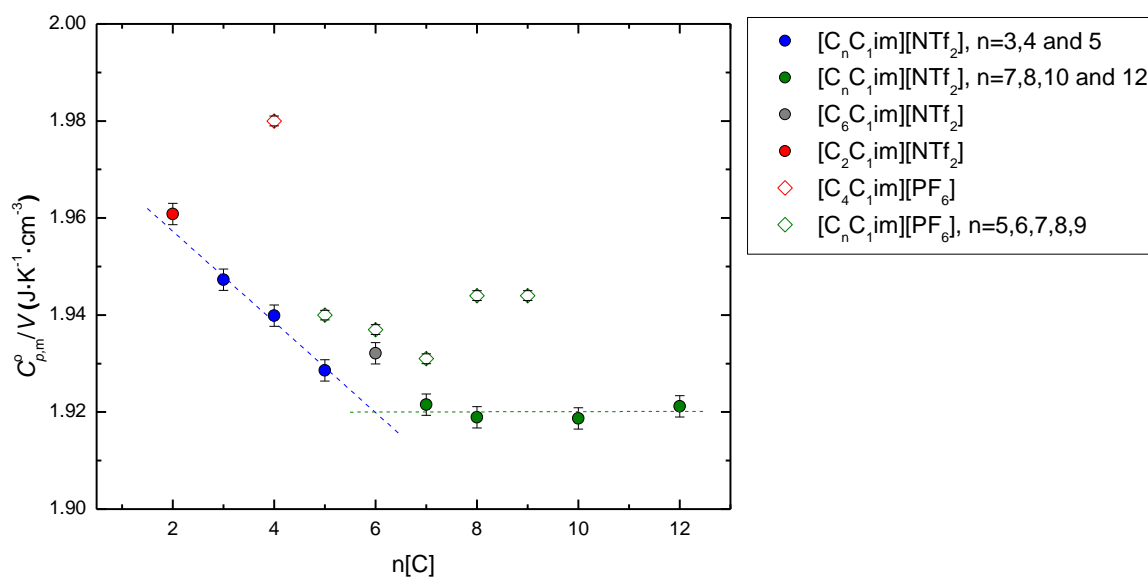
Figure 3.32- Volumic heat capacities at 298 K, as function of the number of carbon atoms in the alkyl side chain of the cation

3.3. Comparison of experimental data with estimation methods

3.3.1. Group contribution methods for phase transitions

In Table 3.11, comparison of experimental glass and melting temperatures obtained in this work with the group contribution method developed by Lazzús [34, 43] for T_g and T_m, represented in eq. 3.5 and 3.6, respectively.

$$T_g(K) = 178.63 + \sum n_i \Delta t_{ci} + \sum n_j \Delta t_{aj} \qquad (3.5)$$

$$T_m(K) = 288.70 + \sum n_i \Delta t_{ci} + \sum n_j \Delta t_{aj} \qquad (3.6)$$

Literature experimental data reported by Chun *et al* [44] is also reported to support the obtained results.

Table 3.11 - T_g and T_m experimental results obtained from [Bnmim][BF$_4$], [Bnmim][PF$_6$], [Bnmim][C$_2$F$_4$HSO$_3$], [Bnmim][NTf$_2$] and [C$_n$C$_1$im][PF$_6$], where n = 2 - 10 and 12. And comparison with the estimated values computed from Lazzús group contribution method [34, 43] and literature data from Chun *et al* [44].

IL	T_g (K)			T_m (K)	
	Calculated	Experimental	Literature[44]	Calculated	Experimental
[Bnmim][BF$_4$]	467.4	235.3	-	360.0	336.5
[Bnmim][PF$_6$]	474.4	244.8	-	335.8	399.7
[Bnmim][C$_2$F$_4$HSO$_3$]	397.4	229.1	-	271.6	315.4
[Bnmim][NTf$_2$]	445.7	216.7	-	-	-
[C$_2$C$_1$im][PF$_6$]	194.0	-	-	357.9	317.0
[C$_3$C$_1$im][PF$_6$]	195.1	-	-	354.2	311.8
[C$_4$C$_1$im][PF$_6$]	196.3	196.0	196.2	350.4	-
[C$_5$C$_1$im][PF$_6$]	197.5	199.2	193.2	346.6	-
[C$_6$C$_1$im][PF$_6$]	198.6	201.7	193.2	342.9	-
[C$_7$C$_1$im][PF$_6$]	199.8	203.5	189.2	339.1	-
[C$_8$C$_1$im][PF$_6$]	200.9	203.5	202.2	335.4	-
[C$_9$C$_1$im][PF$_6$]	202.1	205.9	207.2	331.6	293.0
[C$_{10}$C$_1$im][PF$_6$]	203.2	208.2	-	327.8	307.1
[C$_{12}$C$_1$im][PF$_6$]	205.6	-	-	324.1	326.5

Calculated values for [Bnmim] series are highly influenced by the values for benzyl (274.990 K) and for SO_2^- (-759.500 K) which the author, Lazzús [34, 43] confirmed. Those values deeply influence the results computed (notice that for if a IL with SO_2^-, it is impossible to possess a positive melting temperature or glass transition) and do not allow an accordance with the values for the experimental data obtained.

Obtained results are, in general, in agreement with the estimated values with exception of [Bnmim] T_g values where the value for benzyl group seems rather high and influences the T_g values computed for this set of compounds. It was also observed that the T_g and the heat capacities, in compounds such as ILs, increase with the number of atoms in the alkyl chain, in accordance with Paulechka [45].

In Table 3.12, another GCM was used, from Gharagheizi et al [46, 47], but the T_g (computed through eq. 3.7 for T_g and eq. 3.8 for T_m) values are not in accordance with the experimental data. Also, there is a big lack of groups and when a group is presented, evaluation is very difficult due rather complex definitions presented in the paper by Gharagheizi et al [46, 47], which can easily lead to error.

$$T_g(K) = 158.87 + \sum n_i \Delta t_{ci} + \sum n_j \Delta t_{aj} \tag{3.7}$$

$$T_m(K) = 264.29 + \sum n_i \Delta t_{ci} + \sum n_j \Delta t_{aj} \tag{3.8}$$

Table 3.12 - T_g and T_m experimentally obtained for [Bnmim][BF$_4$], [Bnmim][PF$_6$], [Bnmim][C$_2$F$_4$HSO$_3$], [Bnmim][NTf$_2$] and the estimated values from Gharagheizi et al [46, 47] GCM.

IL	T_g (K)		T_m (K)	
	Computed	Experimental	Calculated	Experimental
[Bnmim][BF$_4$]	-	235.3	-	336.5
[Bnmim][PF$_6$]	-	244.8	-	399.7
[Bnmim][C$_2$F$_4$HSO$_3$]	289.8	229.1	311.9	315.4
[Bnmim][NTf$_2$]	335.1	216.7	-	-

3.3.2. Group contribution method for heat capacities

In Table 3.13 are presented the heat capacities for the $[C_nC_1im]$ series, at 298.15 K, and show the influence of the alkyl chain growth in the heat capacity. The experimental data was compared with the group contribution method (GCM) by Gardas *et al* [27] represented in eq. 3.9.

$$C_p(T/K) = R[A + B(T/100) + D(T/1000)^2]$$ (3.9)

And literature data from Paulechka (for C_4C_1) [45].

Table 3.13 - Experimental molar heat capacity data, at 298 K, obtained for $[C_nC_1im][PF_6]$, where *n* = 2 - 10 and 12, and comparison with Gardas *et al* [27] group contribution method and literature data from Paulechka [45].

$[C_nC_1im][PF_6]$	C_p exp (J·K⁻¹·mol⁻¹)	C_pGCM (J·K⁻¹·mol⁻¹)	$C_p$literature (J·K⁻¹·mol⁻¹)
$[C_2C_1im][PF_6]$	346.9 ± 0.2	343.6	-
$[C_3C_1im][PF_6]$	377.5 ± 0.4	375.6	-
$[C_4C_1im][PF_6]$	411.6 ± 0.9	407.6	408.1
$[C_5C_1im][PF_6]$	435.6 ± 0.1	439.6	-
$[C_6C_1im][PF_6]$	467.4 ± 0.1	471.6	-
$[C_7C_1im][PF_6]$	498.9 ± 0.1	503.6	-
$[C_8C_1im][PF_6]$	534.8 ± 0.0	535.6	-
$[C_9C_1im][PF_6]$	567.7 ± 0.1	567.6	-
$[C_{10}C_1im][PF_6]$	600.8 ± 12.8	599.6	-
$[C_{12}C_1im][PF_6]$	659.5 ± 2.0	663.6	-

In figure Figure 3.33 presents the experimental results and the comparison with the GCM computed values presented by Gardas *et al* [27] and a literature value. C_2, C_4, C_{10} and C_{12} are solids at 298 K. For those ILs, the liquid heat capacities, at 298 K, were derive by linear extrapolation from the liquid region of the experimental data.
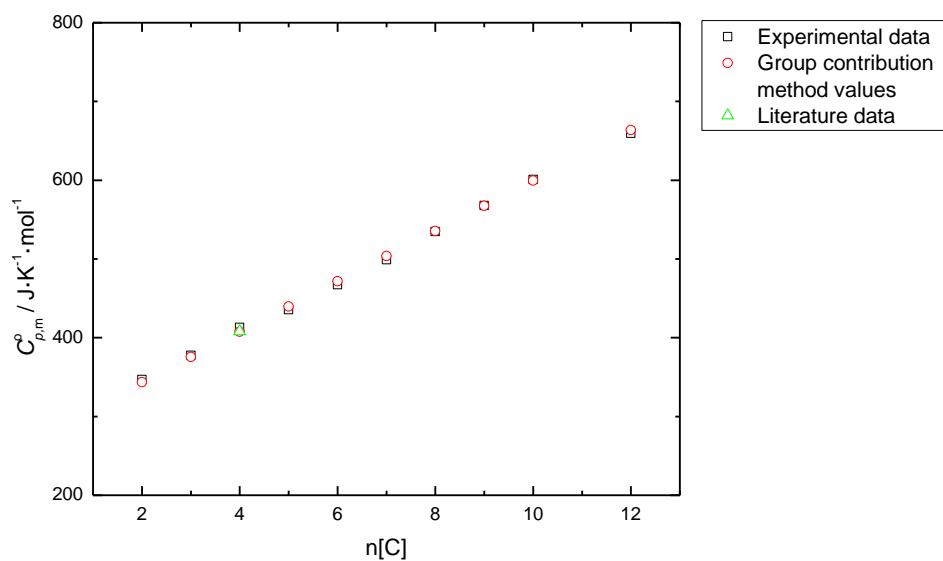
Figure 3.33 - Comparison between the data obtained for $[C_nC_1im][PF_6]$, where n = 2 - 10 and 12, and the data from group contribution method and literature data found for the same compounds.

In Figure 3.34 is presented the relative deviation of the experimental values from the GCM values. The graphic show good correlation between experimental values and GCM computed values.
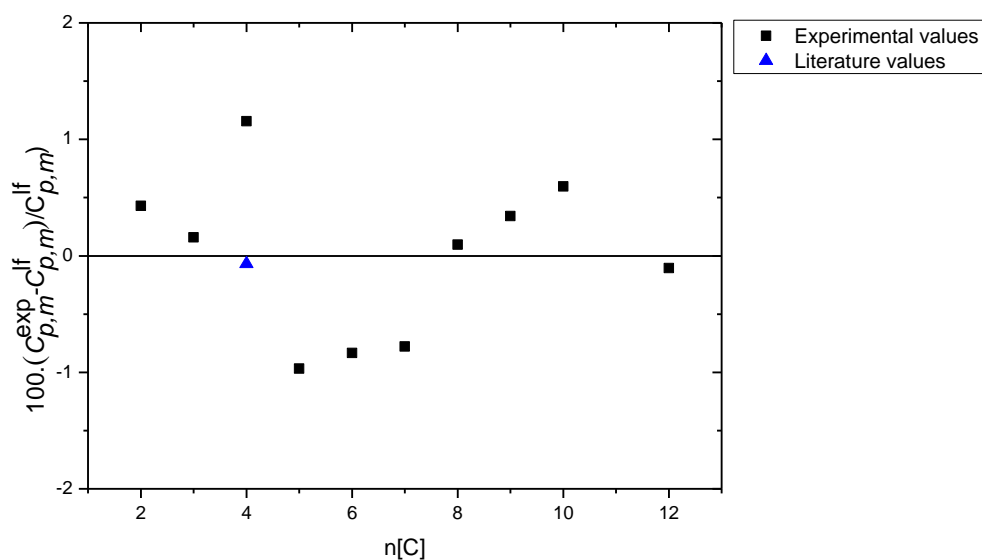
Figure 3.34 – Relative deviation from GCM values (0 line), of the experimental and literature values for $[C_nC_1im][PF_6]$, where n = 2 - 10 and 12. "0 line" stands for the values obtained by linear fit.

4. Conclusions

This work was focused on the thermal study, condensed phases heat capacities measurements and phase behaviour studies of ionic liquids. Two families were studied. One based on the 1-benzyl-3-methylimidazolium cation conjugated with 4 anions (tetrafluoroborate; hexafluorophosphate; 1,1,2,2-tetrafluoroethanesulfonate; bis(trifluoromethylsulfonyl)imide), and one based in the 1-alkyl-3-methylimidazolium series: -methyl; -ethyl; -propyl; -butyl; -pentyl; -hexyl; –heptyl; -octyl; -nonyl; -decyl and -dodecyl-3-methylimidazolium with the anion hexafluorophosphate. A comparative analysis for the anion effect in the 1-benzyl-3-methylimidazolium ionic liquids, and the benzyl group effect was performed, as well as the alkyl side chain length effect on the properties of 1-alkyl-3-methylimidazolium series.

The thermal phase behaviour study was carried out in the temperature range 183 to 423 K, and compared with available literature values as well as with group contribution estimation methods.

The results from TA Instruments Q1000 DSC were compiled and shown in Table 3.1 and the ratio T_g/T_m was calculated. The T_g/T_m ratio of the [Bnmim][PF$_6$] the was found to be outside the typical [2/3 to 3/4] range.

Experimental glass transition temperatures T_g obtained in this work are well predicted by the method of Lazzús [34, 43] where it can be found that for 1-alkyl- 3-methylimidazolium, T_g results are typically in the region between 183 K and 203 K in accordance with Holbrey *et al* [48]. For melting temperatures T_m the deviations from the prediction by GCM is significantly due to the particular effect of the structuration and nanostructuration of the ILs in the relative stability between crystal and the liquid phases. From the thermal behaviour results of the PF6 series, some indication was found concerning the relation between the solid-solid transition temperature, T_{s-s}, and the appearance of the cool crystallization temperature T_{cc}. The thermal analysis profile of studied ILs series could be divided in two distinct regions/behaviours. The region is characterized by a small decrease in the T_m and T_{s-s}, along the alkyl side chain, and starting from [C$_7$C$_1$im][PF$_6$] an increase of the T_m and T_{s-s} is observed with the alkyl side chain length in agreement with the trend shift recently reported in the literature for several physicochemical properties along the ILs series [39, 42].

Condensed state heat capacities data are reported, in the temperature range 258 to 355 K, and compared with available literature values as well as with group contribution estimation methods.

Since the data in the literature for the studied ILs is scarce, estimation methods were used to support experimental data. The experimental heat capacities are quite well predicted by the Gardas *et al* [27] group contribution method.

5. References

1.   Noack, K., et al., *The role of the C2 position in interionic interactions of imidazolium based ionic liquids: a vibrational and NMR spectroscopic study.* Physical Chemistry Chemical Physics, 2010. **12**(42): p. 14153-14161.

2.   Tokuda, H., et al., *How Ionic Are Room-Temperature Ionic Liquids? An Indicator of the Physicochemical Properties.* The Journal of Physical Chemistry B, 2006. **110**(39): p. 19593-19600.

3.   Marisa A. A. Rocha, J.A.P.C., Luís M. N. B. F. Santos, *Evidence of Nanostructuration from the Heat Capacities of the 1,3-dialkylimidazolium bis(trifluoromethylsulfonyl)imide Ionic Liquid Series.*

4.   Pringle, J.M., et al., *Physical trends and structural features in organic salts of the thiocyanate anion.* Journal of Materials Chemistry, 2002. **12**(12): p. 3475-3480.

5.   Shimizu, K., et al., *Three commentaries on the nano-segregated structure of ionic liquids.* Journal of Molecular Structure: THEOCHEM, 2010. **946**(1–3): p. 70-76.

6.   Troncoso, J., et al., *Thermodynamic properties of imidazolium-based ionic liquids: densities, heat capacities, and enthalpies of fusion of [bmim][PF6] and [bmim][NTf2].* J. Chem. Eng. Data, 2006. **51**(5): p. 1856-1859.

7.   Diedrichs, A. and J. Gmehling, *Measurement of heat capacities of ionic liquids by differential scanning calorimetry.* Fluid Phase Equilib., 2006. **244**(1): p. 68-77.

8.   Goharshadi, E.K. and M. Moosavi, *Thermodynamic properties of some ionic liquids using a simple equation of state.* Journal of Molecular Liquids, 2008. **142**(1–3): p. 41-44.

9.   Wang, H., et al., *Friction and wear behaviors of ionic liquid of alkylimidazolium hexafluorophosphates as lubricants for steel/steel contact.* Wear, 2004. **256**(1–2): p. 44-48.

10.   B. Wu, R.G.R., and R. D. Rogers, *Solar Energy: The Power to Choose.* Proceedings of Solar Forum 2001.

11.   D. Holbrey, J. and K. R. Seddon, *The phase behaviour of 1-alkyl-3-methylimidazolium tetrafluoroborates; ionic liquids and ionic liquid crystals.* Journal of the Chemical Society, Dalton Transactions, 1999. **0**(13): p. 2133-2140.

12. Zhou, Y. and M. Antonietti, *Synthesis of Very Small TiO2 Nanocrystals in a Room-Temperature Ionic Liquid and Their Self-Assembly toward Mesoporous Spherical Aggregates.* Journal of the American Chemical Society, 2003. **125**(49): p. 14960-14961.

13. Armstrong, D.W., et al., *Ionic Liquids as Matrixes for Matrix-Assisted Laser Desorption/Ionization Mass Spectrometry.* Analytical Chemistry, 2001. **73**(15): p. 3679-3686.

14. Andre, M., et al., *Ionic Liquids as Advantageous Solvents for Headspace Gas Chromatography of Compounds with Low Vapor Pressure.* Analytical Chemistry, 2004. **77**(2): p. 702-705.

15. Yanes, E.G., et al., *Capillary Electrophoretic Application of 1-Alkyl-3-methylimidazolium-Based Ionic Liquids.* Analytical Chemistry, 2001. **73**(16): p. 3838-3844.

16. Scovazzo, P., et al., *Gas separations using non-hexafluorophosphate [PF6]− anion supported ionic liquid membranes.* Journal of Membrane Science, 2004. **238**(1–2): p. 57-63.

17. Jork, C., et al., *Influence of Ionic Liquids on the Phase Behavior of Aqueous Azeotropic Systems.* Journal of Chemical & Engineering Data, 2004. **49**(4): p. 852-857.

18. Uerdingen, M., *Entschwefelung von Dieselkraftstoff.* Chemie in unserer Zeit, 2004. **38**(3): p. 212-213.

19. Fortunato, R., et al., *Supported liquid membranes using ionic liquids: study of stability and transport mechanisms.* Journal of Membrane Science, 2004. **242**(1–2): p. 197-209.

20. Haines, P.J., *Principles of Thermal Analysis and Calorimetry* RSC Paperbacks

21. G. W. H. Höhne, W.F.H., H.-J. Flammersheim *Differential Scanning Calorimetry 2nd edition.* Springer.

22. *Laboratory for Emerging Materials and Technology.* http://www.clemson.edu/ces/lemt/TA%20Q1000%20DSC.htm, (accessed February 15th, 2013)

23. Straka, M., K. Růžička, and V. Růžička, *Heat Capacities of Chloroanilines and Chloronitrobenzenes.* Journal of Chemical & Engineering Data, 2007. **52**(4): p. 1375-1380.

24. Fulem, M., et al., *Heat Capacities of Tetracene and Pentacene.* Journal of Chemical & Engineering Data, 2008. **53**(9): p. 2175-2181.

25. Atkins, P.W.D.P.J.A.P.W., *Atkins' Physical chemistry.* 2006, New York: W.H. Freeman.

26. McQuarrie, D.A.S.J.D., *Physical chemistry : a molecular approach.* 1997, Sausalito, Calif.: University Science Books.

27. Gardas, R.L. and J.A.P. Coutinho, *A Group Contribution Method for Heat Capacity Estimation of Ionic Liquids.* Ind. Eng. Chem. Res., 2008. **47**(15): p. 5751-5757.

28. Papon, P., J. Leblond, and P.E. Meijer, *Phase Transitions in Liquids and Solids: Solidi.cation and Melting*, in *The Physics of Phase Transitions*, P. Papon, J. Leblond, and P.E. Meijer, Editors. 2006, Springer Berlin Heidelberg. p. 79-124.

29. Wellen, R.M.R. and M.S. Rabello, *The kinetics of isothermal cold crystallization and tensile properties of poly(ethylene terephthalate).* Journal of Materials Science, 2005. **40**(23): p. 6099-6104.

30. MacFarlane, D.R., et al., *Structural studies of ambient temperature plastic crystal ion conductors.* Journal of Physics: Condensed Matter, 2001. **13**(36): p. 8257.

31. Lobland, *The nature of the glassy state: structure and glass transitions.* Journal of Materials Education. **34**: p. p. 69 - 94.

32. Castner, J.E.W. and J.F. Wishart, *Spotlight on ionic liquids.* The Journal of Chemical Physics, 2010. **132**(12): p. 120901-9.

33. Yu, X., et al., *Correlation between the glass transition temperatures and multipole moments for polymers.* Chemical Physics, 2007. **332**(1): p. 115-118.

34. Lazzús, J.A., *A group contribution method to predict the glass transition temperature of ionic liquids.* Thermochimica Acta, 2012. **528**(0): p. 38-44.

35. Haida, O., H. Suga, and S. Seki, *Calorimetric study of the glassy state XII. Plural glass-transition phenomena of ethanol.* The Journal of Chemical Thermodynamics, 1977. **9**(12): p. 1133-1148.

36. Dierking, I., *Book Review: The Physics of Phase Transitions: Concepts and Applications. By Pierre Papon, Jacques Leblond, and Paul H. E. Meijer.* ChemPhysChem, 2003. **4**(4): p. 401-402.

37. Dean, P.M., J.M. Pringle, and D.R. MacFarlane, *Structural analysis of low melting organic salts: perspectives on ionic liquids.* Physical Chemistry Chemical Physics, 2010. **12**(32): p. 9144-9153.

38. M. E. Wieser, M.B., Pure Appl. Chem. , 2009. **81**.

39. Rocha, M.A.A., J.A.P. Coutinho, and L.M.N.B.F. Santos, *Evidence of nanostructuration from the heat capacities of the 1,3-dialkylimidazolium bis(trifluoromethylsulfonyl)imide ionic liquid series.* The Journal of Chemical Physics, 2013. **139**(10): p. 104502-5.

40. Miguel Vilas, M.A.A.R., Emilia Tojo, Luís M. N. B. F. Santos, *Novel 1-Ethyl-2-Alkylpyridinium based Ionic Liquids: Synthesis and Volatility.* Chemistry - A European Journal.

41. Rocha, M.A.A., et al., *Heat capacities at 298.15 K of the extended [CnC1im][Ntf2] ionic liquid series.* J. Chem. Thermodyn., 2012. **53**: p. 140-143.

42. M. A. A. Rocha, F.M.S.R., J. A. P. Coutinho, Luís M. N. B. F. Santos,, *Heat Capacities at 298.15 K of [CN-1C1im][PF6] Ionic Liquids Series.* J. Mol. Liq. (submitted), 2013.

43. Lazzús, J.A., *A group contribution method to predict the melting point of ionic liquids.* Fluid Phase Equilibria, 2012. **313**(0): p. 1-6.

44. Chun, S., S.V. Dzyuba, and R.A. Bartsch, *Influence of Structural Variation in Room-Temperature Ionic Liquids on the Selectivity and Efficiency of Competitive Alkali Metal Salt Extraction by a Crown Ether.* Analytical Chemistry, 2001. **73**(15): p. 3737-3741.

45. Paulechka, Y.U., *Heat Capacity of Room-Temperature Ionic Liquids: A Critical Review.* Journal of Physical and Chemical Reference Data, 2010. **39**(3).

46. Gharagheizi, F., P. Ilani-Kashkouli, and A.H. Mohammadi, *A group contribution method for estimation of glass transition temperature ionic liquids.* Chemical Engineering Science, 2012. **81**(0): p. 91-105.

47. Gharagheizi, F., P. Ilani-Kashkouli, and A.H. Mohammadi, *Computation of normal melting temperature of ionic liquids using a group contribution method.* Fluid Phase Equilibria, 2012. **329**(0): p. 1-7.

48.	Holbrey, J.D., et al., *Physicochemical Properties*, in *Ionic Liquids in Synthesis*. 2008, Wiley-VCH Verlag GmbH & Co. KGaA. p. 57-174.